Sustainable and Resilient Hydrogen Supply Chain Planning under Uncertainty: A Stochastic Multi-Period Case Study of the Marmara Region

Abdullah Zübeyr Şekerci * , Selin Soner Kara , Şule Itır Satoğlu

Posted Date: 23 April 2026

doi: 10.20944/preprints202604.1696.v1

Keywords: hydrogen supply chain; stochastic optimization; energy transition; disaster resilience; multi-period planning; variable neighborhood search

 doi:10.20944/preprints202604.1696.v1

Article

Sustainable and Resilient Hydrogen Supply Chain Planning under Uncertainty: A Stochastic Multi-Period Case Study of the Marmara Region

Abdullah Zübeyr Şekerci [1,2,*], Selin Soner Kara [1] and Şule Itır Satoğlu [2]

[1] Faculty of Mechanical Engineering, Industrial Engineering Department, Yildiz Technical University, Besiktas 34349, Istanbul, Turkey

[2] Faculty of Management, Industrial Engineering Department, Istanbul Technical University, Istanbul 34367, Turkey

* Correspondence: abdullahzsekerci@gmail.com

Abstract

Hydrogen (H_2) is regarded as a promising option for sustainable energy systems; however, its large-scale use in electricity supply remains limited. This study develops a stochastic network optimization model to examine the applicability of H_2-based electricity generation. The proposed Hydrogen Supply Chain (HSC) model evaluates cost and emission performance under uncertainty by considering disaster conditions, transmission losses, depreciation, and the time value of money. The Marmara Region of Türkiye is divided into 24 grid nodes, and a single-period model for 2023 is solved using Mixed-Integer Linear Programming (MILP). The HSC is allowed to meet 10–40% of electricity demand and to replace collapsed grid lines by supplying critical public centers (CPCs) during disasters. The results show that the HSC can meet about 25% of demand, although at costs higher than power grid (PG) electricity, while keeping emissions near zero. The model is then extended to a multi-period structure (2023–2053) and solved by Variable Neighborhood Search (VNS). Over time, H_2 costs decline, and its share rises from 19% to 35%. These findings suggest that H_2 can support long-term sustainability, resilience, and energy security.

Keywords: hydrogen supply chain; stochastic optimization; energy transition; disaster resilience; multi-period planning; variable neighborhood search

1. Introduction

The continuous increase in global energy demand and the necessity to combat climate change are accelerating the transition from fossil fuel–based energy systems to RES worldwide. This transformation is driven not only by environmental concerns but also by objectives related to energy supply security and economic sustainability. Roadmaps published by the International Energy Agency (IEA) and similar institutions recommend restructuring national energy systems in line with carbon neutrality and sustainable development targets, and many countries have begun implementing these policies accordingly [1,2].

To examine the current global situation, the graph presented in Figure 1 presents electricity generation and energy consumption levels according to their respective energy sources.

 doi:10.20944/preprints202604.1696.v1

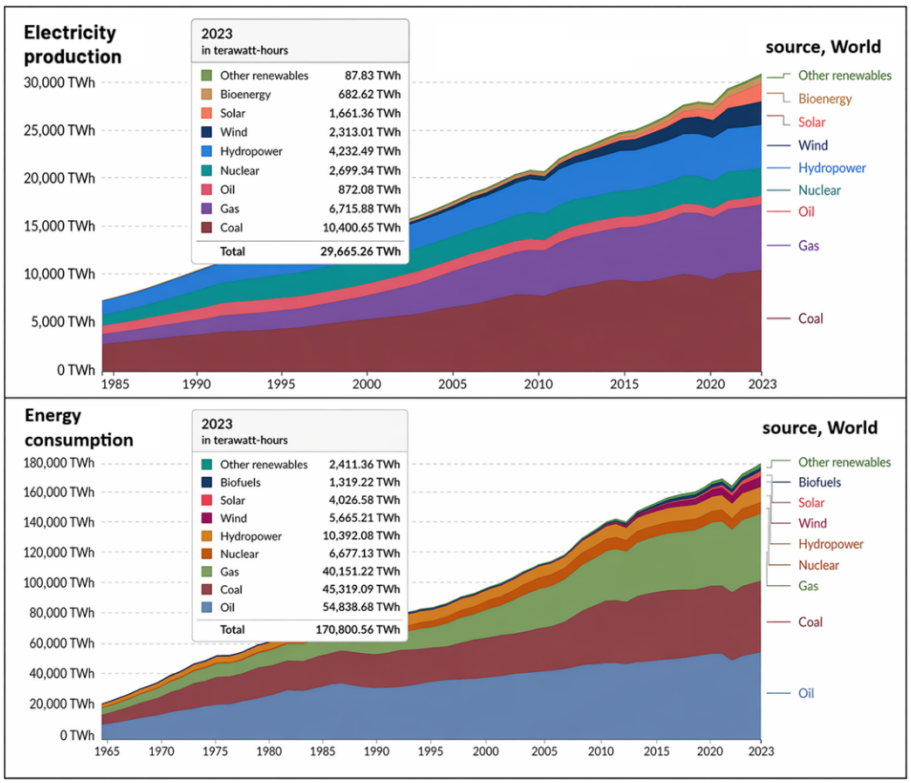

*Other renewables (electricity production): include geothermal, wave, and tidal.

**Other renewables (energy consumption): geothermal, biomass, H_2, waste energy.

Figure 1. Electricity production and energy consumption values according to sources/World.

When energy consumption and electricity generation data are examined, it is evident that global energy demand is still largely met by fossil fuels. A significant portion of total primary energy consumption consists of oil, coal, and natural gas, although the share of RES has been steadily increasing [3]. It is noteworthy that the fastest growth within RES -also the focus of this study - has occurred in electricity generation; wind and solar energy have reached a substantial share of electricity production, particularly over the past decade, contributing to more sustainable energy systems.

From a country- and region-based perspective, Figure 1 shows that when nuclear sources (NS) are included, the global share of RES in electricity generation is approximately 37%, whereas it is about 31% when only direct RES are considered. In the European Union (EU), these figures are approximately 61% and 39%, respectively, both exceeding the global average. Long-standing policy measures have reduced the share of fossil fuels (FS) while largely maintaining nuclear generation at stable levels. In the United States, although the share including NS is above the global average at around 40%, the direct RES share remains near 22%. The continued reliance on fossil fuels limits the expected decline in carbon emissions [4].

In China, despite growth in RES capacity, the dominance of coal has kept the share at approximately 35% NS and about 30% direct RES, and emissions have not declined significantly. India remains below the global average, with shares of approximately 23% NS and 21% direct RES; despite targets to expand solar energy, fossil fuel dependence constrains the increase in RES share [5].

While global RES investments are rapidly increasing, the transition becomes more critical in developing economies with growing energy demand. In this context, Türkiye—despite not yet having nuclear generation—exceeds the global average with a direct RES share of approximately 42% [6]. Since a substantial portion of national energy consumption occurs in the Marmara Region,

 doi:10.20944/preprints202604.1696.v1

characterized by dense industry and population, the region represents a priority area for energy transition initiatives from a sustainability perspective.

Within this transition process, H_2 - considered nearly emission-free - stands out. Although its cost remains high and its practical use remains limited, leading to predominantly theoretical studies within the RES domain, it offers distinctive advantages. Beyond its near-zero emissions profile, H_2 functions both as an energy source and as an energy carrier. Its diverse applications and regional utilization patterns are illustrated in Figure 2.

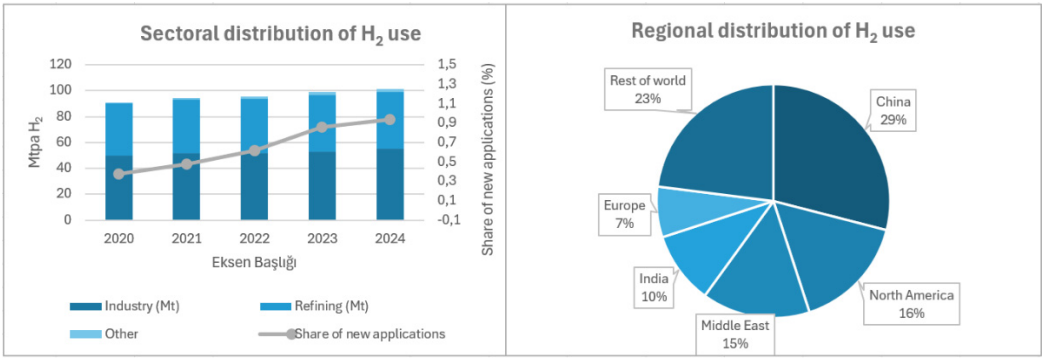

*Other: transport, production of H_2-based fuels, power generation, buildings and biofuels upgrading

Figure 2. H2 use by sector and region / worldwide.

As illustrated in Figure 2, the majority of H_2 use occurs as an energy carrier in industry and refineries. In industrial applications, it is used as a feedstock in the production of ammonia and methanol, while in refineries it serves primarily as a refining agent; together, these applications account for nearly 90% of total H_2 utilization, constituting the energy carrier component. In contrast, H_2 is used as a fuel in power systems such as gas turbines and fuel cells (FCs), representing approximately 10% of total usage and forming the energy component. In this context, the current global consumption of H_2 is around 100 Mt, remaining relatively low [7,8].

In light of the above considerations, despite its currently limited share in energy applications, H_2 offers several strategic advantages compared to other renewable energy alternatives. Unlike intermittent sources such as wind and solar, it can store energy over longer periods and allows production and consumption to be separated. It can also be transported, stored at scale, and converted into electricity when needed, making it useful for balancing supply and demand. In addition, compared to conventional grid-based systems, H_2-based solutions can operate independently of transmission infrastructure, which becomes especially important in disruption scenarios. These characteristics make H_2 not only a complementary energy carrier but also a practical option for improving system reliability and supporting sustainable energy transitions, supporting its selection as the study focus [1,2].

In this context, this study develops a single-period and a multi-period HSC model to assess the usability of H_2 through cost and emission analyses. The model incorporates key real-world factors such as depreciation, transmission losses, efficiency, the time value of money, and inventory conditions. Although data limitations exist, parameters are compiled from the literature and international sources.

The Marmara Region of Türkiye is divided into 24 grid nodes based on its industrial and population structure, and 2023 electricity demand is assigned accordingly. CPCs are also defined for each grid with additional demand under disaster conditions.

The system follows an H_2 production–storage–distribution structure, where H_2 is transported, converted into electricity via FCs, and injected into the grid. The HSC is allowed to supply 10%, 20%, 30%, 40% of regional demand, and its impact is evaluated in terms of costs and emissions.

Results of the single-period stochastic MILP model (24 scenarios) show that HSC supplies about 25% of demand, with costs around four times higher than grid electricity but negligible emissions.

 doi:10.20944/preprints202604.1696.v1

For future analysis, the model is extended to 2023–2053 with 10 periods and 240 scenarios. Due to its size, the model is solved using the VNS metaheuristic, and produces near-optimal results. Over time, H_2 shifts toward RES-based technologies, costs decrease to about twice grid electricity, and HSC utilization increases. To the best of the authors' knowledge, this is the first study that simultaneously develops a multi-period stochastic HSC model, integrates FC–based electricity supply, and considers disaster resilience within a sustainable energy planning framework.

The remainder of the paper is organized as follows. Section 2 reviews the literature. Section 3 presents the methodological flow, the mathematical model, and the VNS algorithm. The application for the Marmara Region of Türkiye and the results are presented, followed by discussion and conclusion.

Beyond its methodological contribution, this study is also motivated by policy needs related to energy transition and resilience planning. In particular, the model aims to support decision-makers in evaluating the role of H_2 within regional electricity systems under uncertainty. Rather than focusing solely on system optimization, the study seeks to identify how different H_2 penetration levels, technology choices, and infrastructure investments affect long-term cost, emission, and reliability outcomes.

From a policy perspective, this framework provides a basis for assessing trade-offs between economic feasibility and environmental sustainability, as well as the potential role of H_2 systems in supporting critical infrastructure during disruption scenarios. In this sense, the model is designed not only as an analytical tool but also as a decision-support framework for long-term energy planning.

2. Literature Review

Early studies on the use of H_2 as an energy carrier emerged in the 1970s. However, applications remained limited for a long time due to high costs and technological constraints. With growing environmental concerns of the 2000s and advancements in renewable energy technologies, research on HSCs has gained momentum.

Hugo et al. [9] developed a multi-objective optimization model for H_2 infrastructure planning, highlighting the trade-offs between investment cost and environmental impacts. Kim et al. [10] incorporated demand uncertainty within a stochastic framework for South Korea, demonstrating that uncertainty significantly affects network design. Similarly, Almansoori and Shah [11] proposed a scenario-based stochastic model for the United Kingdom, covering the entire supply chain, from production to distribution. Zhang and Jiang [12] emphasized the importance of environmental criteria in China's H_2 network design, while Ogumerem [13] demonstrated a balance between sustainability and profitability through the use of electrolysis by-products. Woo et al. [14] focused on cost optimization in biomass-based H_2 production, identifying the importance of import and inventory decisions. Silva et al. [15] introduced modeling flexibility through a multi-scenario model for Brazil, and achieved cost reductions under demand variability. Ehrenstein [16] evaluated H_2 transition within planetary boundaries, and Almaraz et al. [17] further expanded the scope by integrating economic, environmental, and social dimensions. Many of these studies adopted multi-period frameworks to capture long-term system evolution. In contrast, Yu et al. [18] demonstrated that alternative transport and storage options, such as organic liquids, can reduce emissions, where carbon taxation plays a critical role in network design. In this context, the HSC literature is summarized in Table 1, including information on the authors, publication years, and model characteristics.

Table 1. Literature review of HSC studies.

Writer(s)	Year	Application*	Demand Category**	Objective formulation***	Objective type	Uncertainty Type ****	Time Horizon
Hugo et al. [9].	2005	HSC$^{G. Britain}$	MV	max-p	MULTI	DET	MULTI
Kim et al. [10]	2008	HSC$^{S. Korea}$	RD	min-c	SINGLE	DET	MULTI
Kamarudin et al. [19]	2009	HSC^{Malaysia}	MV	min-c	SINGLE	DET	SINGLE
Gosálbez et al.. [20]	2010	HSC$^{G. Britain}$	MV	min-c	MULTI	DET	MULTI
Almansoori ve Shah [11]	2012	HSC$^{G. Britain}$	MV	min-c	SINGLE	STO	MULTI
Johnson ve Ogden [21]	2012	HSC^{USA}	RD	min-c	SINGLE	DET	MULTI
Zhang ve Jiang [12]	2015	RSC^{China}	RD	min-c, min-e	MULTI	DET	SINGLE
Woo [14]	2016	HSC$^{S. Korea}$	MV	min-c	SINGLE	DET	SINGLE
Won et al. [22]	2017	HSC$^{S. Korea}$	MV	min-c	SINGLE	DET	SINGLE
Ogumerem [13]	2018	HSC^{USA}	MV	max-p	MULTI	DET	MULTI
Ayvaz et al. [23]	2018	RSC^{Türkiye}	MV	min-c	SINGLE	DET	MULTI
Talebian [24]	2019	HSC^{Canada}	MV	min-c	SINGLE	DET	MULTI
Silva et al. [15]	2021	HSC^{Brazil}	RD	min-c	SINGLE	STO	MULTI
Manier et al. [25]	2020	HSC^{France}	MV	min-c	SINGLE	DET	MULTI
Ehrenstein [16]	2020	HSC^{UK}	RD	min-c, min-e	MULTI	DET	SINGLE
Güler et al. [26]	2021	HSC^{Türkiye}	MV	min-c, min-e, min-sr	MULTI	DET	MULTI
Almaraz et al. [17]	2022	HSC^{Hungary}	ID & MV	min-c	MULTI	DET	SINGLE
Forghani et al. [27]	2023	HSC^{Oman}	RD	min-c, min-e	MULTI	DET	MULTI
Doniavi et al. [28]	2023	HSC^{Iranian}	ID	min-c	SINGLE	DET	MULTI
Ibrahim & Al-Mohannadi [29]	2023	HSC^{Qatar}	ID	min-c, min-e	MULTI	DET	MULTI
Sgarbossa et al. [30]	2023	HSC^{Europe}	MV	min-c, min-e	MULTI	DET	MULTI
Yu et al. [18]	2025	HSC^{China}	RD	min-c	SINGLE	DET	MULTI
Hou et al. [31]	2025	HSC$^{Green H2}$	RD	min-c	SINGLE	STO	SINGLE
This study	202-	HSC^{Türkiye}	RD & DA	min-c, min-e	MULTI	STO	MULTI

*RSC: Renewable supply chain. **MV: Mobil vehicles, RD: Regional demand, ID: Industrial demand, DA: Disaster area. ***max-p: maximum profit, min-e: minimum enviromental effect, min-c: minimum cost, min-sr: minimum security risk. ****DET: Deterministic, STO: Stochastic.

 doi:10.20944/preprints202604.1696.v1

While the existing literature provides valuable contributions to H_2 supply chain design, several differences distinguish this study. Most previous works focus on hydrogen supply for transportation or industrial applications and often end the analysis at the delivery stage without explicitly modeling final energy use [9,11,13,14]. In contrast, this study considers hydrogen-to-electricity conversion and evaluates system performance at the point of end use within the PG. In addition, although stochastic and multi-period approaches are used in some studies [10,11,15,18], the combined treatment of uncertainty, long-term system evolution, and disaster resilience is still limited. This study addresses these gaps by developing a multi-period stochastic framework that also includes a resilience-oriented design, where hydrogen-based electricity can supply critical public centers during disruptions. Furthermore, while some studies examine environmental and economic trade-offs [9,12,16,17], they generally do not link these aspects to grid-level electricity supply and system resilience within a single framework. Therefore, the proposed model provides a more comprehensive assessment by jointly considering cost structures, emission dynamics, infrastructure decisions, and resilience requirements.

The main contributions of this study are summarized as follows:

- Most HSC studies focus on transportation or industrial uses and do not model final energy use. This study incorporates hydrogen-to-electricity conversion and grid-level supply.
- A disaster-resilient framework is proposed, enabling hydrogen-based electricity to operate independently of the grid and supply CPCs.
- The model integrates key real-world factors (e.g., time value of money, losses, efficiencies), improving realism and applicability.
- A stochastic structure captures uncertainty in demand, system performance, and disaster conditions.
- A multi-period framework (2023–2053) models long-term investment and technological transitions.
- A VNS metaheuristic is employed to solve the large-scale multi-period stochastic model.

The methodological progression of the study is presented in the following section.

3. Methodology and Model Construction

This section presents the methodology of the study, is organized into three subsections. The first subsection describes the methodological flow of the study, the second outlines the model assumptions, and the third presents the mathematical model.

3.1. Methodological Flow

The model addressed in this study performs both single-period and multi-period analyses for the HSC and provides a forward-looking cost-emission assessment. The overall methodological flow illustrating the process of the study is presented in Figure 3.

 doi:10.20944/preprints202604.1696.v1

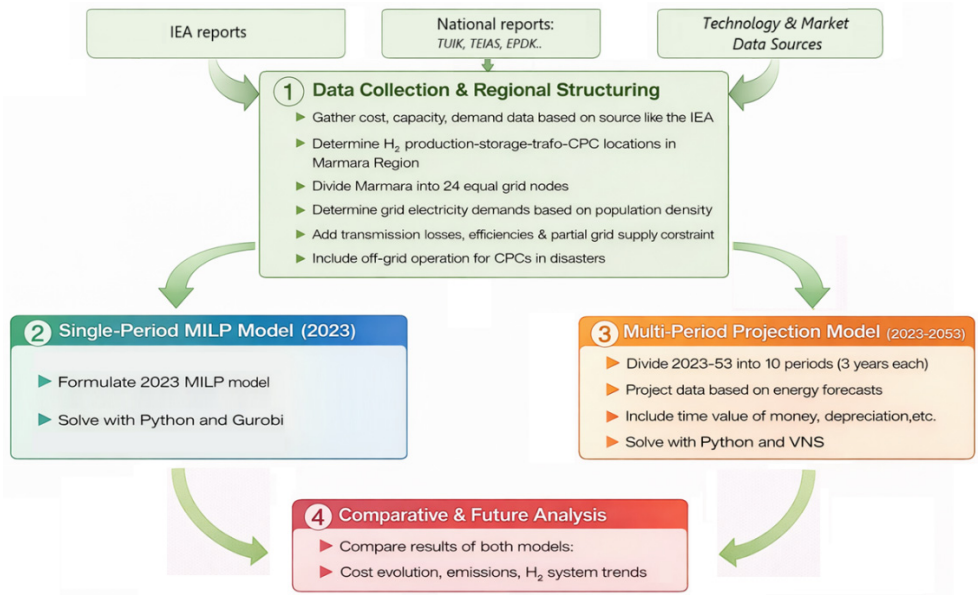

Figure 3. Methodological flow of the HSC model.

The model assumptions, based on the methodological flow presented above, are provided below.

3.2. Model Assumptions

When the HSC model is formulated as a single-period problem, it is solved using MILP. However, when the model is extended to a multi-period structure, its size increases significantly, making it difficult for solvers to find an optimal solutions. Therefore, the VNS approach, which generates approximate solutions through an iterative search process, is employed. In this study, the assumptions and mathematical formulation of the multi-period model, as an extension of the single-period model, are presented. Accordingly, the model assumptions are listed below:

I. The system is modeled as a multi-layer HSC network including production nodes, storage nodes, FC locations, grid demand nodes, and CPCs. Hydrogen flows from production to storage and then to FC units, where electricity is generated.
II. The planning horizon is multi-period, and once installed, facilities remain operational.
III. Hydrogen transport uses predefined modes, with one transport mode selected per connection.
IV. Grid demand is met by either HSC or the main PG, while CPCs are supplied only by the HSC network.
V. CPC nodes become active only under disaster conditions, during which hydrogen-based electricity generation prioritizes the supply of CPC demand.
VI. The HSC network is allowed to supply between 10% and 40% of total grid electricity demand. Transmission efficiency, line losses, and availability factors are incorporated into the network representation.
VII. Investment decisions are subject to budget limitations, and financial factors such as the time value of money and depreciation are incorporated into the model.
VIII. Technology capacities, costs, and performance parameters are projected based on international energy outlooks and technology roadmaps.

3.3. Mathematical Model Formulation

In this section, the structure of the MILP model and the VNS metaheuristic are examined in two separate subsections.

 doi:10.20944/preprints202604.1696.v1

3.3.1. MILP Model Structure

It should be noted that although the single-period model constitutes the core of the multi-period framework, the analysis of the single-period case cannot be directly obtained from the outputs of the multi-period model. Therefore, separate models are constructed for each structure, and the underlying reasons are explained below.

I. First, the single-period model is designed to evaluate the annual unit cost of the HSC network in the Marmara Region. While the single-period formulation optimizes annual costs, the multi-period model extends the planning horizon to 2053, which corresponds to Türkiye's strategic target year for hydrogen development [32]. In this extended framework, the 30-year horizon is divided into ten periods, each representing three years. Therefore, the multi-period structure is examined separately to capture long-term dynamics and investment evolution.

II. Second, when the 24-scenario single-period model is expanded into a 10-period structure, the number of scenarios, parameters, variables, and data increases substantially. As a result, the problem becomes computationally intractable as a pure optimization model. Consequently, the integrated single-model structure is separated, and a distinct multi-period model is established. This large-scale formulation is solved using the VNS metaheuristic.

Given its broader scope, only the mathematical formulation of the multi-period model is presented. In the results section, however, the outputs of both models are analyzed and compared.

Based on the model assumptions presented above, the mathematical formulations of the sets, parameters, decision variables, and objective function of the HSC multi-period model, together with their definitions, are presented below. In this context, Table A1 in the Appendix presents the sets and their definitions, Table A2 provides the parameters and their descriptions, and Table A3 shows the decision variables and their definitions in the model.

Based on the sets, parameters, and decision variables of the MILP model, the objective function is formulated as shown in the following equation. The model minimizes both costs and emissions; however, instead of a multi-objective structure, emissions are incorporated into the objective function through a penalty coefficient λ. In this way, the original multi-objective problem is transformed into a single-objective formulation. The objective function is given in Equation (1).

$$\min Z = \sum_{\beta \in B} DF^{\beta} \left[Cfn^{\beta} + Cax^{\beta} + Cfx^{\beta} + \sum_{\omega \in W} prob_{\omega} (Cg_{\omega}^{\beta} + Ccp_{\omega}^{\beta} + Cvr_{\omega}^{\beta} + \lambda E_{\omega}^{\beta} + Pen_{\omega}^{\beta}) \right] \quad (1)$$

The intermediate cost components expressed as subtotals in the objective function are detailed explicitly in the following equations.

$$DF^{\beta} = \frac{1}{(1+dr)^{(\beta-1)\Delta}} \quad (2)$$

$$Cfn^{\beta} = \sum_{i \in I} \sum_{r \in R} fnP_r^{\beta} \delta_{i,r}^{\beta} + \sum_{s \in S} \sum_{q \in Q} fnS_q^{\beta} \phi_{s,q}^{\beta} + \sum_{k \in K} fnF_k^{\beta} \psi_k^{\beta} \quad (3)$$

Cfn^{β}: It represents the total FOPEN associated with production, storage, and transportation facilities.

$fnP_r^{\beta} \delta_{i,r}^{\beta}$: If technology r is installed at location i, the corresponding fixed capital investment cost for production is incurred.

$fnS_q^{\beta} \phi_{s,q}^{\beta}$: If technology q is installed at location s, the corresponding fixed capital investment cost for storage is incurred.

$fnF_k^{\beta} \psi_k^{\beta}$: If a FC unit is installed at candidate site k during period β, the corresponding fixed investment cost for the FC is incurred.

$$\begin{aligned} Cax^{\beta} = & \sum_{i \in I} \sum_{r \in R} CRFp_r CapP_r^{\beta} \, cxP_r^{\beta} \delta_{i,r}^{\beta} + \sum_{s \in S} \sum_{q \in Q} CRFs_q CapS_q^{\beta} \, cxS_q^{\beta} \phi_{s,q}^{\beta} + \sum_{k \in K} CRFf_k CapF_k^{\beta} \, cxF_k^{\beta} \psi_k^{\beta} \\ & + \sum_{i \in I} \sum_{s \in S} \sum_{t \in T} CRFt_t dPS_{i,s,t} \, cxT_t^{\beta} \gamma_{i,s,t}^{\beta} + \sum_{s \in S} \sum_{k \in K} \sum_{t \in T} CRFt_t dPS_{s,k,t} \, cxT_t^{\beta} \gamma_{s,k,t}^{\beta} \end{aligned} \quad (4)$$

 doi:10.20944/preprints202604.1696.v1

$$CRFp_r^{\beta} = \frac{dr(1+dr)^{Lp_r}}{(1+dr)^{Lp_r}-1} \tag{5}$$

$$CRFs_q^{\beta} = \frac{dr(1+dr)^{Ls_q}}{(1+dr)^{Ls_q}-1} \tag{6}$$

$$CRFf_k^{\beta} = \frac{dr(1+dr)^{Lf_k}}{(1+dr)^{Lf_k}-1} \tag{7}$$

$$CRFt_t^{\beta} = \frac{dr(1+dr)^{Lt_t}}{(1+dr)^{Lt_t}-1} \tag{8}$$

Cax^{β}: It represents the total annualized CAPEX associated with production, storage, and FC facilities in period β.

$CRFp_r^{\beta} CapP_r^{\beta} cxpr_r^{\beta} \delta_{i,r}^{\beta}$: If production technology r is installed at location i, the corresponding annualized CAPEX is incurred. This cost is calculated by multiplying the installed production capacity with the unit investment cost and the capital recovery factor.

$CRFs_q^{\beta} CapS_q^{\beta} cxst_q^{\beta} \phi_{s,q}^{\beta}$: If storage technology q is installed at location s, the corresponding annualized CAPEX for storage is incurred, based on the installed capacity and capital recovery factor.

$CRFf_k^{\beta} CapF_k^{\beta} cxfc_k^{\beta} \psi_k^{\beta}$: If a FC unit is installed at candidate site k, the corresponding annualized CAPEX is incurred, determined by the installed FC capacity and capital recovery factor.

$CRFt_t dPS_{i,s,t} cxt_t^{\beta} \gamma_{i,s,t}^{\beta}$: This represents the annual CAPEX of establishing transportation infrastructure between production point i and storage point s using transportation mode t, provided the relevant transportation link is established.

$CRFt_t dPS_{s,k,t} cxt_t^{\beta} \gamma_{s,k,t}^{\beta}$: This represents the annual CAPEX of establishing transportation infrastructure between storage node s and FC node k using mode t, provided the relevant transportation link is established.

$$Cfx^{\beta} = \sum_{i\in I}\sum_{r\in R} fxP_r^{\beta}\delta_{i,r}^{\beta} + \sum_{s\in S}\sum_{q\in Q} fxS_q^{\beta}\phi_{s,q}^{\beta} + \sum_{k\in K} fxF_k^{\beta}\psi_k^{\beta} \tag{9}$$

Cfx^{β}: It represents the total FOPEX associated with production, storage, and transportation facilities.

$fxP_r^{\beta}\delta_{i,r}^{\beta}$: If technology r is installed at location i, the corresponding FOPEX for production is incurred.

$fxS_q^{\beta}\phi_{s,q}^{\beta}$: If technology q is installed at location s, the corresponding FOPEX cost for storage is incurred.

$fxF_k^{\beta}\psi_k^{\beta}$: If a FC unit is installed at candidate site k during period β, the corresponding FOPEX for the FC is incurred.

$$Cg_{\omega}^{\beta} = \sum_{g\in G} cGR_{\omega}^{\beta} pGR_{g,\omega}^{\beta} \tag{10}$$

Cg_{ω}^{β}: Cost of electricity purchased from the external PG.

$$Ccp_{\omega}^{\beta} = \sum_{k\in K^g}\sum_{t\in T^{road}} \left(cSK_t^{\beta} dGC_{gc}\right) z_{g,c,t,\omega}^{\beta} \tag{11}$$

Ccp_{ω}^{β}: Total VOPEX of hydrogen delivered from grid nodes to CPC nodes under scenario ω during period β (USD/year).

 doi:10.20944/preprints202604.1696.v1

$$Cvr_{\omega}^{\beta} = CvrP_{\omega}^{\beta} + CvrPS_{\omega}^{\beta} + CvrSK_{\omega}^{\beta} \tag{12}$$

Cvr_{ω}^{β}: VOPEX arising from production and transportation.

$$CvrP_{\omega}^{\beta} = \sum_{i\in I}\sum_{r\in R} vP_r^{\beta}\, h_{i,r,\omega}^{\beta} \tag{13}$$

$CvrP_{\omega}^{\beta}$: VOPEX incurred from hydrogen production at production node i using technology r under scenario ω during period β.

$$CvrPS_{\omega}^{\beta} = \sum_{i\in I}\sum_{s\in S}\sum_{t\in T}(cPS_t^{\beta}\, dPS_{i,s,t})x_{i,s,t,\omega}^{\beta} \tag{14}$$

$CvrPS_{\omega}^{\beta}$:Transportation VOPEX of hydrogen shipped from production node i to storage node s using mode t under scenario ω during period β.

$$CvrSK_{\omega}^{\beta} = \sum_{s\in S}\sum_{k\in K}\sum_{t\in T}(cSK_t^{\beta}\, dSK_{s,k,t})y_{s,k,t,\omega}^{\beta} \tag{15}$$

$CvrSK_{\omega}^{\beta}$:Transportation VOPEX of hydrogen delivered from storage node s to FC site k using transport mode t under scenario ω during period β.

$$\begin{aligned} E_{\omega}^{\beta} = {} & \sum_{g} efGR_g^{\beta} pGR_{g,\omega}^{\beta} + \sum_{i,r} efP_r^{\beta} h_{i,r,\omega}^{\beta} + \sum_{i,s,t} efTR_r^{\beta} dPS_{i,s,t} \\ & + \sum_{s,k,t} efTR_r^{\beta} dSK_{s,k,t} + \sum_{k\in K^g,c,t\in T^{road}} (efTR_r^{\beta} dGC_{gc}) z_{g,c,t,\omega}^{\beta} + \sum_{k\in K} efF_k^{\beta} eF_{k,\omega}^{\beta} \end{aligned} \tag{16}$$

E_{ω}^{β}: Total greenhouse gas emissions generated under scenario ω during period β, including production, transportation, PG electricity purchase, and FC generation (tCO_2/year).

- $efGR_g^{\beta} pGR_{g,\omega}^{\beta}$: Grid electricity emissions
- $efP_r^{\beta} h_{i,r,\omega}^{\beta}$: Production emissions
- $efTR_r^{\beta} dPS_{i,s,t}$: Production–storage transport emissions
- $efTR_r^{\beta} dSK_{s,k,t}$: Storage–FC transport emissions
- $(efTR_r^{\beta} dGC_{gc}) z_{g,c,t,\omega}^{\beta}$: Grid–CPC transport emissions
- $efF_k^{\beta} eF_{k,\omega}^{\beta}$: FC generation emissions

$$Pen_{\omega}^{\beta} = pDG \sum_{g\in G} slDG_{g,\omega}^{\beta} + pCPC \sum_{g\in G} slCPC_{g,\omega}^{\beta} + pZLslZL_{\omega}^{\beta} + pZUslZU_{\omega}^{\beta} + pSO \sum_{s\in S} SO_{s,\omega}^{\beta} \tag{17}$$

Pen_{ω}^{β}: Total penalty cost incurred from constraint violations under scenario ω during period β.

- $pDG \sum_{g\in G} slDG_{g,\omega}^{\beta}$: Grid unmet demand penalty
- $pCPC \sum_{g\in G} slCPC_{g,\omega}^{\beta}$: CPC unmet demand penalty
- $pZLslZL_{\omega}^{\beta}$: H_2 share lower violation
- $pZUslZU_{\omega}^{\beta}$: H_2 share upper violation
- $pSO \sum_{s\in S} SO_{s,\omega}^{\beta}$: Penalty for unmet demand due to stockout.

The constraints of the multi-period MILP model are presented and explained in detail below.

Demand constraints;

- *Global H_2 share lower bound*: Ensures that hydrogen-based electricity generation satisfies minimum HSC target share (10%) under each scenario and period.

$$\eta_{\omega}^{\beta} \sum_{k\in K^g}\sum_{g\in G} eGR_{k,g,\omega}^{\beta} + slZL_{g,\omega}^{\beta} \geq \zeta_{\omega}^{\beta} \sum_{g\in G} DG_{\omega}^{\beta} \qquad \forall\omega,\beta \tag{18}$$

- *Global H_2 share upper bound*: Ensures that hydrogen-based electricity generation satisfies maximum HSC target share (40%) under each scenario and period.

 doi:10.20944/preprints202604.1696.v1

$$\eta_{\omega}^{\beta} \sum_{k \in K^{g}} \sum_{g \in G} eGR_{k,g,\omega}^{\beta} \leq \zeta_{\omega}^{\beta} \sum_{g \in G} DG_{\omega}^{\beta} + slZU_{g,\omega}^{\beta} \qquad \forall \omega, \beta \tag{19}$$

- *Grid demand satisfaction*: Ensures grid demand is met by HSC and/or external PG supply, with slack if needed.

$$\eta_{\omega}^{\beta} \left(\sum_{k \in K^{g}} eGR_{k,g,\omega}^{\beta} + pGR_{g,\omega}^{\beta} \right) + slDG_{g,\omega}^{\beta} \geq DG_{\omega}^{\beta} \qquad \forall g, \omega, \beta \tag{20}$$

- Production constraints;
  - *Production capacity constraint*: Restricts hydrogen production at each node by the installed technology capacity adjusted by scenario-based availability.

$$\sum_{r \in R} h_{i,r}^{\beta} \leq aPR_{\omega} \sum_{r \in R} CapP_{r}^{\beta} \delta_{i,r}^{\beta} \qquad \forall i, \omega, \beta \tag{21}$$

  - *Single production technology selection*: Ensures that at most one production technology is installed at each production node.

$$\sum_{r \in R} \delta_{\mathrm{i,r}}^{\beta} \leq 1 \qquad \forall i, \beta \tag{22}$$

  - *Production–shipping balance*: Forces all produced hydrogen to be transported from production nodes to storage facilities.

$$\sum_{s \in S} \sum_{t \in T} x_{i,s,t,\omega}^{\beta} = \sum_{r \in R} h_{i,r}^{\beta} \qquad \forall i, \omega, \beta \tag{23}$$

- Storage Constraints;
  - *Single storage technology selection*: Ensures that at most one storage technology is installed at each storage node.

$$\sum_{q \in Q} \phi_{s,q}^{\beta} \leq 1 \qquad \forall s, \beta \tag{24}$$

  - *Inter-period inventory balance constraint*: This constraint tracks storage inventory over time considering effective inflows, outflows, and storage losses.

$$Inv_{s,\omega}^{\beta} = \left(1 - \sum_{q \in Q} bo_{q}^{\beta} \phi_{s,q}^{\beta} \right) Inv_{s,\omega}^{\beta-1} + \eta_{\omega}^{\beta} \sum_{i \in I} \sum_{t \in T} \eta PS_{t}^{\beta} x_{i,s,t,\omega}^{\beta} - \sum_{k \in K} \sum_{t \in T} y_{s,k,t,\omega}^{\beta} \qquad \forall s, \omega, \beta \geq 1 \tag{25}$$

  - *Initial inventory condition constraint*: This constraint initializes inventory using initial stock, effective inflows, and outflows.

$$Inv_{s,\omega}^{1} = \left(1 - \sum_{q \in Q} bo_{q}^{1} \phi_{s,q}^{1} \right) InvO_{s} + \eta_{\omega}^{1} \sum_{i \in I} \sum_{t \in T} \eta PS_{t}^{1} x_{i,s,t,\omega}^{1} - \sum_{k \in K} \sum_{t \in T} y_{s,k,t,\omega}^{1} \qquad \forall s, \omega \tag{26}$$

  - *Storage capacity constraint*: This constraint ensures stored hydrogen does not exceed capacity, considering availability.

$$Inv_{s,\omega}^{\beta} \leq aST_{\omega} \sum_{q \in Q} CapS_{q}^{\beta} \phi_{s,q}^{\beta} \qquad \forall s, \omega, \beta \tag{27}$$

  - *Soft safety stock constraint*: This constraint enforces a minimum safety stock level at each storage node.

$$Inv_{s,\omega}^{\beta} + SO_{s,\omega}^{\beta} \geq SS_{s}^{\beta} \qquad \forall s, \omega, \beta \tag{28}$$

- Transport Constraints;

 doi:10.20944/preprints202604.1696.v1

- *Production–storage mode linking*: This constraint allows flow only if the transport mode is selected.

$$x_{i,s,t,\omega}^{\beta} \leq MPS_{i,s,t}\gamma_{i,s,t}^{\beta} \qquad \forall i,s,t,\omega,\beta \tag{29}$$

- *Single transport mode selection (PS arc)*: This constraint ensures that at most one transportation mode is selected for each production–storage pair.

$$\sum_{t\in T}\gamma_{i,s,t}^{\beta} \leq 1 \qquad \forall i,s,\beta \tag{30}$$

- *Storage–FC mode linking*: This constraint permits hydrogen flow from storage to FC sites only when the corresponding transport mode is activated.

$$y_{s,k,t,\omega}^{\beta} \leq MPS_{s,k,t}\gamma_{s,k,t}^{\beta} \qquad \forall s,k,t,\omega,\beta \tag{31}$$

- *Single transport mode selection (SK arc)*: This constraint ensures that only one transport mode is selected between each storage node and FC site.

$$\sum_{t\in T}\gamma_{s,k,t}^{\beta} \leq 1 \qquad \forall s,k,\beta \tag{32}$$

- *CPC hydrogen transport and conversion link*: This constraint restricts CPC deliveries to road transport only.

$$z_{g,c,t,\omega}^{\beta} = 0 \qquad \forall g,c,\omega,\beta, \qquad \forall t \in (T\backslash T^{road}) \tag{33}$$

- FC Constraints;
  - *FC conversion constraint*: This constraint limits electricity generation based on delivered hydrogen, accounting for transport losses and FC efficiency.

$$eF_{k,\omega}^{\beta} \leq \alpha^{\beta}\eta F_{k}^{\beta}\sum_{s\in S}\sum_{t\in T}\eta SK_{t}^{\beta}y_{s,k,t,\omega}^{\beta} \qquad \forall k,\omega,\beta \tag{34}$$

  - *Grid-side electricity dispatch constraint*: Ensures that electricity supplied from a grid-side FC does not exceed its total generation.

$$\sum_{g\in G} eGR_{k,g,\omega}^{\beta} \leq eF_{k,\omega}^{\beta} \qquad \forall k \in K^{g},\omega,\beta \tag{35}$$

  - *FC capacity and installation constraint*: This constraints restricts FC electricity generation by installed capacity and ensures zero generation if no FC is installed.

$$eF_{k,\omega}^{\beta} \leq aFC_{\omega}CapF_{k}^{\beta}\psi_{k}^{\beta} \qquad \forall k,\omega,\beta \tag{36}$$

  - *CPC-side FC installation constraint*: This constraint defines CPC electricity supply as the direct conversion of hydrogen delivered to CPC nodes via local FCs.

$$eCPC_{c,\omega}^{\beta} = \alpha^{\beta}\sum_{g\in G}\sum_{t\in T^{road}} z_{g,c,t,\omega}^{\beta} \qquad \forall c,\omega,\beta \tag{37}$$

- Disaster Related Constraints;
  - *CPC enabled only under disaster*: This constraint allows electricity supply to CPC nodes only when a disaster scenario is active.

$$eCPC_{c,\omega}^{\beta} \leq dis_{\omega}^{\beta}Me \qquad \forall c,\omega,\beta \tag{38}$$

  - *CPC demand satisfaction*: This constraint allows electricity supply to CPC nodes only when a disaster scenario is active.

$$\sum_{c\in C}\mu_{cg}eCPC_{c,\omega}^{\beta} + slCPC_{g,\omega}^{\beta} \geq \mathrm{dis}_{\omega}^{\beta}\sum_{c\in C}\mu_{cg}DC_{c}^{\beta} + \qquad \forall g,\omega,\beta \tag{39}$$

 doi:10.20944/preprints202604.1696.v1

- Investment and Financial Constraints;
  - *Budget constraint*: This constraint ensures that total cost for production, storage, and FC installations in each period do not exceed the budget.

$$\sum_{i,r} cxP_r^{\beta}\delta_{i,r}^{\beta} + \sum_{s,q} cxS_q^{\beta}\phi_{s,q}^{\beta} + \sum_{k} csF_k^{\beta}\psi_k^{\beta} \le BD^{\beta} \qquad \forall\beta \tag{40}$$

  - *Production investment continuity*: This constraint ensures that once a production technology is installed, it cannot be removed in later periods.

$$\delta_{i,r}^{\beta} \ge \delta_{i,r}^{\beta-1} \qquad \forall i,r,\beta > 1 \tag{41}$$

  - *Storage investment continuity*: This constraint ensures that once a storage technology is installed, it cannot be removed in later periods.

$$\phi_{s,q}^{\beta} \ge \phi_{s,q}^{\beta-1} \qquad \forall s,q,\beta > 1 \tag{42}$$

  - *FC investment continuity*: This constraint ensures that once a FC technology is installed, it cannot be removed in later periods.

$$\psi_k^{\beta} \ge \psi_k^{\beta-1} \qquad \forall k,\beta > 1 \tag{43}$$

The MILP formulation is presented above, and the VNS methodology is described next.

3.3.2. VNS Structure

Metaheuristic approaches are widely used for large-scale combinatorial problems where exact methods become computationally demanding. Among these, Variable Neighborhood Search (VNS) stands out for its ability to explore the solution space through multiple neighborhood structures. By systematically applying different neighborhood operators, VNS investigates various regions of the search space and identifies improved solutions with reasonable computational effort [33].

The effectiveness of VNS stems from the fact that a solution locally optimal under one neighborhood may be improved under another. Accordingly, the algorithm alternates between predefined neighborhoods, updating the current solution whenever an improvement is found; otherwise, the algorithm proceeds to the next structure. This iterative process enables VNS to escape local optima and continue the search for better solutions [34].

In this context, if a feasible solution of the VNS method applied to the HSC model is represented by x, which denotes the network configuration throughout all planning periods and includes decisions related to the following:

- Installation of hydrogen production facilities,
- selection of production technologies,
- installation of storage facilities and storage technologies,
- installation of FC units,
- selection of transportation modes between network components

Accordingly, this solution can be represented as

$$x = \left\{x_{i,\beta}^{prod}, x_{i,\beta}^{prod}, x_{k,\beta}^{FC}, r_{i,\beta}, q_{s,\beta}, t_{i,s,\beta}^{PS}, t_{s,k,\beta}^{SK}, t_{k,c,\beta}^{KC}\right\} \qquad \forall g,\omega,\beta \tag{44}$$

where the binary variables $x_{i,\beta}^{prod}$, $x_{i,\beta}^{prod}$, and $x_{k,\beta}^{FC}$ indicate whether a production facility, storage facility, or FC unit is installed at location i, s, or k in period β, respectively. The variables $r_{i,\beta}$ and $q_{s,\beta}$ denote selected production and storage technologies, while $t_{i,s,\beta}^{PS}$, $t_{s,k,\beta}^{SK}$, and $t_{k,c,\beta}^{KC}$ represent transportation mode selections between the corresponding network layers.

The search aims to minimize system cost while penalizing emissions and infeasibility; the fitness function used in the VNS algorithm can be expressed as

$$f(x) = C(x) + \lambda E(x) + Pen(x) \tag{45}$$

where

 doi:10.20944/preprints202604.1696.v1

- $C(x)$ represents the total discounted cost (investment, operation, transport),
- $E(x)$ denotes the total emissions generated by the system,
- $Pen(x)$ represents penalty terms for infeasible or undesirable configurations,
- λ is the emission penalty coefficient.

The VNS algorithm explores multiple neighborhoods of the current solution, each representing a different network modification. Assuming that $N_k(x)$ represents the k-th neighborhood structure of the solution x, these can be shown as follows:

$$k = 1,2,3,4$$
$$N_k(x) = \{x' | \, x' \text{ is generated from x using neighborhood } k\} \quad (46)$$

Accordingly, four neighborhood structures are defined in this study:

- $\boldsymbol{N_1}$ -*Facility opening neighborhood*: This neighborhood randomly activates new production, storage, or FC facilities in a selected planning period.
- $\boldsymbol{N_2}$ -*Technology modification neighborhood*: This neighborhood changes the technology type assigned to an already installed production or storage facility.
- $\boldsymbol{N_3}$ -*Transport mode change neighborhood*: This neighborhood modifies transportation modes between production–storage, storage–FC, or FC–demand nodes.
- $\boldsymbol{N_4}$ -*Diversification neighborhood*: This neighborhood introduces additional FC installations to increase solution diversity and help escape local optima.

The general structure of the proposed VNS algorithm is presented in Algorithm 1:

Algorithm 1. Proposed Variable Neighborhood Search (VNS) Framework

Input Model sets and parameters, penalty coefficients, maximum runtime T_{max}
Output Best solution x^*
Generate an initial network configuration xxx using the initialization procedure.
Evaluate the fitness value $f(x)$ based on system cost, emissions, and penalty terms.
Set the current best solution $x^* \leftarrow x$.
while the stopping criterion is not satisfied **do.**
  for *k=1,2,3,4* **do**
    Generate a candidate solution x' from the neighborhood $N_k(x^*)$.
    Compute the fitness value $f(x')$
    if $f(x') < f(x^*)$ **then**
      Update the best solution $x^* \leftarrow x'$.
        Restart the search from the first neighborhood.
    end
  end
end
Return x^*

Algorithm 1 starts by generating an initial feasible HSC network and evaluating it using the objective function, including costs, emissions, and penalties. The search process explores different neighborhood structures by generating candidate solutions. If an improved solution is identified, it replaces the current solution and the search restarts; otherwise, the next neighborhood is examined. The process continues until a stopping criterion, such as a maximum runtime or a limit on non-improving iterations, is reached.

Algorithm 2, describing the neighborhood search and solution process, is presented below.

Algorithm 2. Neighborhood Generation and Solution Evaluation

Input Current solution x, neighborhood index k.
Output Candidate solution x' and fitness value $f(x')$.
Copy the current solution $x' \leftarrow x$.
Randomly select a planning period β.
if $k = 1$ **then**
Apply the **facility opening neighborhood** by activating a new production, storage, or FC facility.
else if $k = 2$ **then**
Apply the **technology modification neighborhood** by changing the production or storage technology.
else if $k = 3$ **then**
Apply the **transport mode neighborhood** by modifying the transportation mode between network nodes.

 doi:10.20944/preprints202604.1696.v1

6	**else if** $k = 4$ **then** Apply the **diversification neighborhood** by opening an additional FC unit.
7	Enforce carry-forward continuity of installed facilities across planning periods.
8	Evaluate the candidate solution using the fitness function $f(x) = C(x) + \lambda E(x) + Pen(x)$
Return	x' *and* $f(x)$

Algorithm 2 describes the neighborhood generation and evaluation procedure. Candidate solutions are created by modifying the current configuration through predefined neighborhoods, including facility opening, technology changes, transport mode selection, and diversification. Investment continuity across periods is enforced, and each candidate is evaluated based on costs, emissions, and feasibility penalties before being returned to the VNS framework. The evaluated solution is returned to the main VNS framework for comparison with the current best solution.

Figure 4 presents the methodological flow of the VNS-based HSC model.

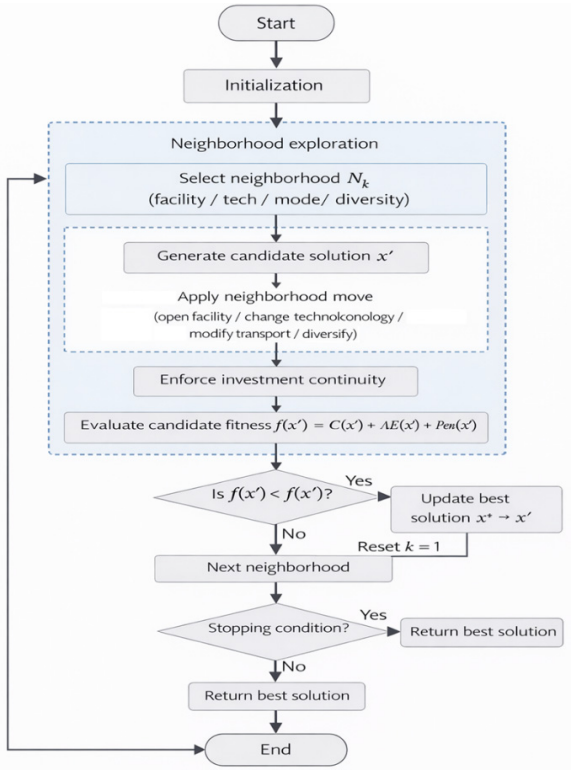

Figure 4. Methodological flow of the VNS model.

Following the model assumptions and mathematical formulations presented above, the application and results are discussed in the following section.

4. Application

In this section, the data related to the parameters used in the single-period and multi-period models, the conceptual structure of the optimization network for the Marmara Region, as well as the results and model comparisons are presented.

4.1. HSC Network and Grid Requirements on the Marmara Region Map

First, regional demand must be determined, which requires identifying the type of final customer of the HSC network. In the literature, H_2 is generally delivered either directly to hydrogen-powered vehicles without being converted into electricity or represented as flows that are supplied to the general grid without a clearly defined final user. In this study, however, a new receiver–transmission configuration that may contribute to the literature is considered. H_2 arriving from

 doi:10.20944/preprints202604.1696.v1

distribution nodes is converted into electricity through FCs assumed to be located adjacent to central transformers within the grid and is then transmitted to the grid line. The electricity produced by the HSC network and integrated into the existing PG at the specified percentages mentioned above thus becomes usable for all types of electricity consumption, including residential, commercial, and industrial uses. The electricity demand for the specified final customers is obtained from the 2023 regional electricity demand data provided by the Turkish Electricity Transmission Corporation (TEİAŞ) [37]. It should be noted that this demand is not distributed on a provincial basis but rather through a grid-based division of the region. This approach is adopted because TEİAŞ performs electricity distribution based on area-based demand allocation. In this distribution, the population, industry, public institutions, and private sector consumption within a given area are all taken into account. In this context, the region is divided into 24 equal-area grid nodes to ensure full regional coverage while keeping the problem size manageable. Figure 5 shows the grid demands and the heat map generated accordingly.

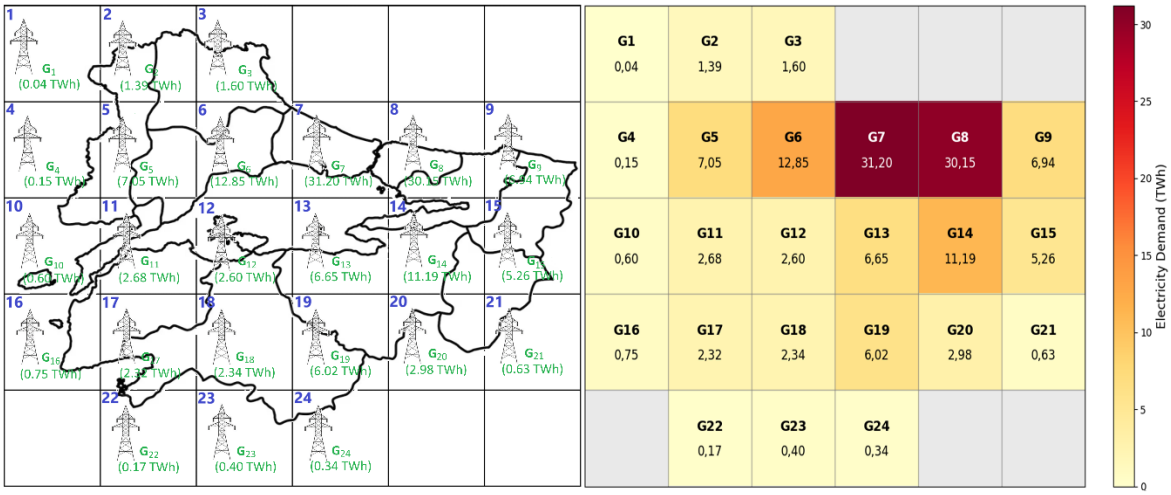

Figure 5. Regional grid electricity demands and heat map.

Another point to note is that the assumption of locating the transformer at the center of the grid is not far from practical applications. Although transformers may not always be exactly at the grid center, they exist within each grid and their distance from the grid center is negligible. In some grids, the distance from the distribution node to the grid center may be greater than the distance to the actual transformer, while in others it may be smaller. Therefore, when all grids are considered collectively, the small differences between the grid-center transformer assumption and actual transformer locations effectively cancel out.

Production and storage nodes must be determined for the HSC network established to meet a portion of the regional demand shown in Figure 5. For production locations, organized industrial zones (OIZ), which are large areas already allocated for industrial production in the Mar-mara Region, are considered. Among the 91 OIZs located in 11 cities in the region, 26 potential production nodes are identified based on characteristics such as city popula-tion, area size, and the number of industrial parcels [35]. For storage locations, indust-rial ports are evaluated, as commonly considered in both the literature and practical applications. The Rotterdam H_2 Hub Port project, the Kobe H_2 Port planned between Australia and Japan, and the Hamburg H_2 Port provide examples demonstrating the suitability of port locations for hydrogen storage [7]. Accordingly, seven ports are se-lected as potential storage locations from among approximately 40 ports around the Marmara Region that can be considered industrial ports [36]. However, in order to enable hydrogen to reach inland areas of the region more effectively, the candidate lo-cations are not limited to coastal ports. Therefore, four additional potential storage lo-cations are defined near production facilities, particularly within organized industrial zones (OIZs). In this way, the storage infrastructure covers both coastal logistics

 doi:10.20944/preprints202604.1696.v1

hubs and inland industrial clusters, resulting in a total of eleven candidate storage locations. It should also be noted that the number of production and storage facilities is intentio-nally limited, since hydrogen production is assumed to contribute only 10–40% of the existing electricity PG supply, and this level of capacity is considered sufficient. In this context, Figure 6 shows the Marmara Region HSC production–distribution–transformer network prepared using Google Maps.

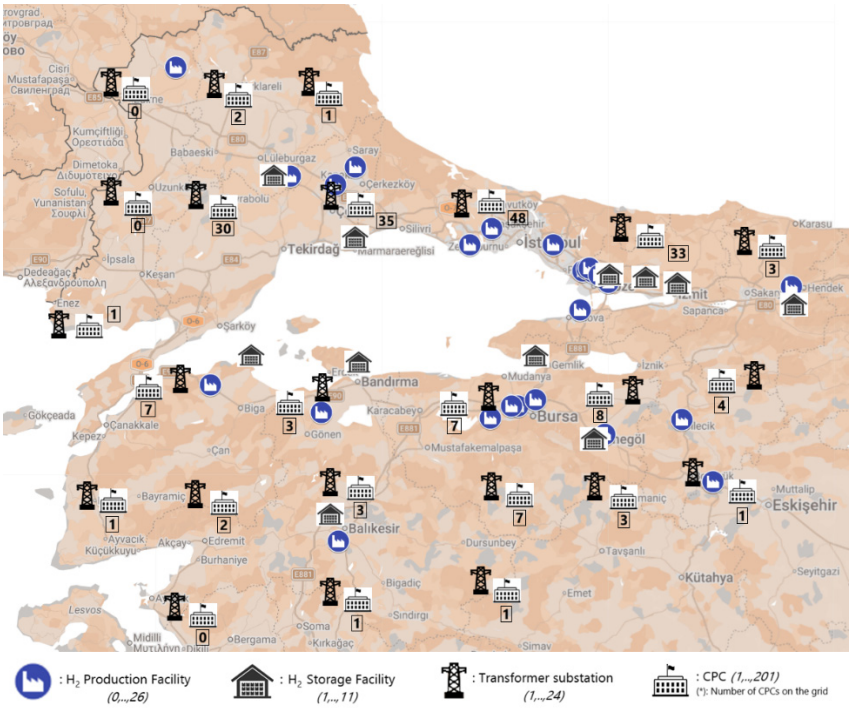

Figure 6. HSC nodes in the Marmara Region on the map.

As shown in Figures 5 and 6, the total electricity demand of the Marmara Region for the year 2023 is determined as 136.3 TWh [37]. This total demand is distributed among the grids according to the population and industrial density of each area, as explained above. Accordingly, the production–distribution system is designed to serve these grids.

In addition, one of the contributions of this study to the literature is the provision of electricity to CPCs through the Hydrogen Supply Chain (HSC) network in disaster situations, as illustrated in Figure 6. The units located around transformer centers and represented as public buildings on the map, with numbers indicating their quantities, correspond to facilities where people can take shelter during disasters. These CPCs are selected in each grid in proportion to the grid population, and a FC unit is positioned adjacent to each CPC.

The main objective is to replace the existing electricity PG, which is assumed to be disrupted during a disaster, by supplying electricity entirely through the HSC network to these facilities. In this system, a portion of the hydrogen delivered to the transformer located at the grid center is transported—without being used within the grid—via road-gas or road-liquid transportation modes to the CPCs. At the CPC locations, hydrogen is converted into electricity through the adjacent FCs.

Within the entire network, 24 FC units are located at the grid centers and 201 FC units are located at the CPCs, resulting in a total of 225 FCs. While Figure 5 illustrates the geographical node locations of the network on the map, Figure 6 presents the flow structure of the HSC network.

 doi:10.20944/preprints202604.1696.v1

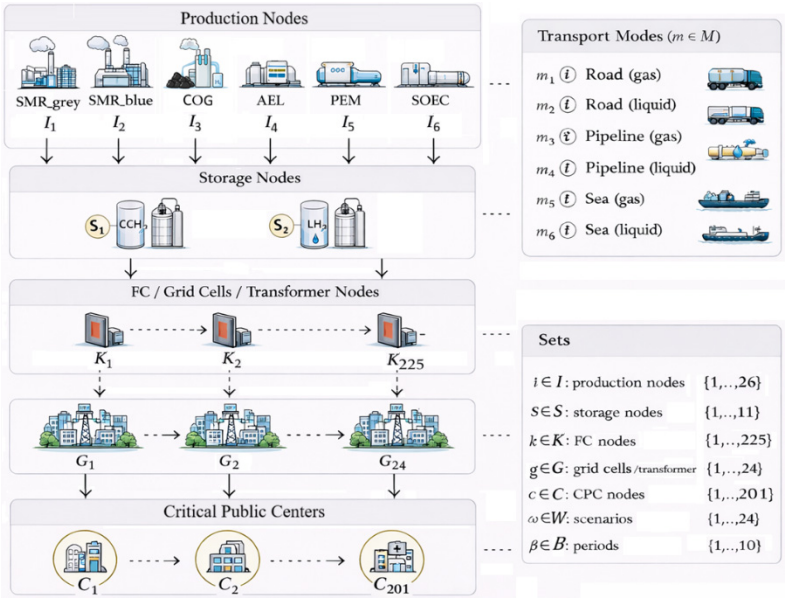

Figure 7. Representative flow structure of the HSC network.

The data related to the production and distribution units included in the flow above, along with information on their projections, are presented in the next subsection.

4.2. Information About the HSC Network

In this section, first, the capacity and cost information of the production, storage, FC (FC), and transportation modes are presented in tabular form. The characteristics of these modes and their future projections are then examined. Subsequently, information regarding scenario components, emissions, and economic parameters is also provided in tables. In this context, Table 2 first presents the data related to the production and distribution system.

Table 2. Cost, emission and efficiency data for production, storage, and FC nodes.

Paramater*	Production Tech						unit	Storage Tech		unit	FC Tech	unit
	SMR_g	SMR_b	COG	AEL	PEM	SOEC		CGH_2	LH_2		PEM	
FOPEN	350	450	550	250	390	300	*million $/site*	60	80	*million $/site*	5	*million USD/site*
FOPEX	30	44	46	32	52	80	*USD/kW*	0.08	0.02	*USD/kgH_2*	15	*USD/kW*
CAPEX	700	1150	1000	850	1000	2600	*USD/kW*	1.65	1.44	*USD/kgH_2*	900	*USD/kW*
VOPEX	1.00	1.40	2.20	1.20	0.85	0.70	*USD /kgH_2*	-	-	*USD/kgH_2*	-	*USD/kgH_2*
Capacity	550	510	500	480	330	175	*million kgH_2*	500	460	*million kgH_2*	3000	*million kWh*
Elec. conv.	0.80	1.00	2.00	52	55	40	*kWh/kgH_2*	-	-	*kWh/kgH_2*	-	-
Alpha (α^{β})	-	-	-	-	-	-	-	-	-	-	20.5	*kWh/kgH_2*
Efficiency (ηF_k^{β})	-	-	-	-	-	-	-	-	-	-	0.60	*rate*
Emission	9.5	1.2	15	0.1	0.05	0.03	*kgCO_2/kgH_2*	0.01	0.02	*kgCO_2/kgH_2*	0.00	*000kgCO_2/ kWh*

*Some of the costs and electrical conversion definitions are given in the previous parameter table, Table 2, while those not in cluded in Table 2 are specified in the following energy calculation equation. *The data presented in Table 2 are compiled from international energy reports (e.g., IEA) [1,2,38–40] relevant literature, and technology roadmaps, and are harmonized and calibrated for model consistency.

H_2 production technologies are expected to evolve significantly between 2023 and 2053. Conventional pathways such as SMR_g are mature and widely deployed but have limited cost reduction potential and high carbon intensity, reducing long-term competitiveness. SMR_b may serve as a transitional option through carbon capture and storage (CCS) despite higher costs, while coal gasification is likely to lose competitiveness in low-carbon systems due to high lifecycle emissions.

 doi:10.20944/preprints202604.1696.v1

In contrast, electrolysis-based technologies are projected to achieve stronger cost reductions driven by technological learning and renewable energy integration. AEL, as the most mature electrolysis technology, is expected to experience gradual cost declines, while PEM offers higher operational flexibility and is likely to benefit from scaling and material improvements. SOEC, although less mature, presents the highest long-term potential due to its high efficiency and ability to utilize waste heat, which may enable more significant cost reductions compared to AEL and PEM [38,39].

Regarding storage, CGH_2 remains the most mature and reliable option with gradual cost improvements, whereas LH_2, despite higher complexity and energy requirements, is expected to gain importance for large-scale and long-distance applications as cryogenic technologies advance [38,40].

On the demand side, PEM FCs are considered a promising solution for electricity generation, particularly in decentralized and critical applications, with expected cost reductions driven by technological improvements and mass production [38,41].

These cost components are commonly used in the technical-economic analysis of hydrogen and are based on the Levelized Cost of Hydrogen (LCOH), which is used in the literature for general energy cost calculations. To show the cost trajectories of hydrogen production technologies between 2023-53, a period-specific LCOH formulation is used:

$$LCOH_r^{\beta} = \frac{CRFp_r(FixedOpen_r^{\beta} + Capex_r^{\beta} Cap_r^{\beta})}{H_r^{\beta}} + \frac{FixedOpex_r^{\beta} Cap_r^{\beta}}{H_r^{\beta}} + VarOpex_r^{\beta} + Elec_r^{\beta} Pel^{\beta} \quad (46)$$

where;

- $LCOH_r^{\beta}$: Levelized hydrogen cost value in period β of r technology.
- Pel^{β}: Electricity unit price during period β.
- H_r^{β}: The amount of hydrogen produced in period β.

Based on the 2023 cost data presented in Table 2 and the comparative analysis of technology development projections derived from various energy agencies, cost projections up to 2053 have been generated. In this process, the LCOH formulation defined above has been applied to each technology to derive period-specific values. In this context, Figure 8 illustrates the cost evolution of production, storage, and FC (FC) technologies between 2023 and 2053.

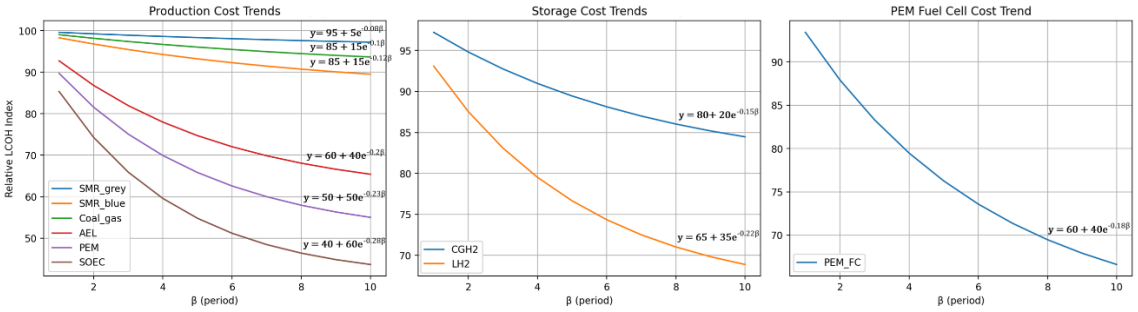

Figure 8. Cost projection 2023-53 for H_2 production-storage-FC Technologies.

The data and cost projections for the production–distribution network nodes are presented. The data corresponding to the transportation nodes, which ensure the connections between these nodes, are provided in Table 3.

Table 3. Cost, emission and efficiency data for transportation nodes.

Parameter	Transportation Modes						unit
	Road_liq	Road_gas	Pipe_liq	Pipe_gas	Sea_liq	Sea_gas	
P-S* distance FOPEN cost	12500	10000	140000	120000	25000	20000	*USD/(kgH₂.km)*
S-K distance FOPEX cost	6000	4000	80000	50000	12000	8000	*USD/(kgH₂.km)*
P-S distance VOPEX cost	0.0008	0.0010	0.00025	0.0003	0.0005	0.0006	*USD/(km.year)*

 doi:10.20944/preprints202604.1696.v1

S-K distance VOPEX cost	0.0007	0.0007	0.0002	0.0002	0.00045	0.0005	*USD/(km.year)*
P-S Efficiency (ηPS_t^{β})	0.985	0.96	0.99	0.995	0.99	0.97	*rate*
S-K Efficiency (ηSK_t^{β})	0.985	0.96	0.99	0.995	0.99	0.97	*rate*
Emission	0.0004	0.00055	0.00018	0.00028	0.00024	0.00036	$gCO_2/(kgH_2.km)$

*P-S: Production-Storage nodes, S-K: Storage-FC nodes. *Transport parameters in Table 3 are based on literature and the U.S. DOE HDSAM [42–44], and are calibrated for model consistency.

Table 3 presents the cost per kilometer between nodes according to transport modes, along with their efficiency and emission characteristics.

In addition, since the information related to grid nodes is extensively used in the model, these data are also presented in tabular form. As stated above, electricity demand and emissions are determined based on the population and industrial density of each grid region, and the corresponding values are provided in Table 4.

Table 4. Grid (and CPC) demands, electricity purchased, emission datas.

Grid Nodes	Electricity Demand	unit	CPC Demand	unit	Grid Electricity Purchased	unit	Emission	unit
G_1	0,040	*MWh*	0,000	*MWh*	35,62	*$/MWh*	0,0197	$kgCO_2/kWh$
G_2	1,386	*MWh*	0,004	*MWh*	36,30	*$/MWh*	0,0201	$kgCO_2/kWh$
G_3	1,597	*MWh*	0,003	*MWh*	36,41	*$/MWh*	0,0201	$kgCO_2/kWh$
G_4	0,149	*MWh*	0,001	*MWh*	35,67	*$/MWh*	0,0197	$kgCO_2/kWh$
G_5	6,972	*MWh*	0,078	*MWh*	39,14	*$/MWh*	0,0216	$kgCO_2/kWh$
G_6	12,759	*MWh*	0,091	*MWh*	42,09	*$/MWh*	0,0233	$kgCO_2/kWh$
G_7	31,078	*MWh*	0,122	*MWh*	51,42	*$/MWh*	0,0281	$kgCO_2/kWh$
G_8	30,060	*MWh*	0,090	*MWh*	50,90	*$/MWh*	0,0279	$kgCO_2/kWh$
G_9	5,933	*MWh*	0,007	*MWh*	38,62	*$/MWh*	0,0214	$kgCO_2/kWh$
G_{10}	0,598	*MWh*	0,002	*MWh*	35,90	*$/MWh*	0,0199	$kgCO_2/kWh$
G_{11}	2,662	*MWh*	0,018	*MWh*	36,95	*$/MWh*	0,0204	$kgCO_2/kWh$
G_{12}	2,592	*MWh*	0,008	*MWh*	36,92	*$/MWh*	0,0204	$kgCO_2/kWh$
G_{13}	6,631	*MWh*	0,019	*MWh*	38,97	*$/MWh*	0,0216	$kgCO_2/kWh$
G_{14}	11,171	*MWh*	0,019	*MWh*	41,28	*$/MWh*	0,0227	$kgCO_2/kWh$
G_{15}	5,250	*MWh*	0,010	*MWh*	38,27	*$/MWh*	0,0212	$kgCO_2/kWh$
G_{16}	0,749	*MWh*	0,001	*MWh*	35,98	*$/MWh*	0,0199	$kgCO_2/kWh$
G_{17}	2,325	*MWh*	0,005	*MWh*	36,78	*$/MWh*	0,0203	$kgCO_2/kWh$
G_{18}	2,332	*MWh*	0,008	*MWh*	36,78	*$/MWh*	0,0203	$kgCO_2/kWh$
G_{19}	6,003	*MWh*	0,017	*MWh*	38,65	*$/MWh*	0,0214	$kgCO_2/kWh$
G_{20}	2,973	*MWh*	0,007	*MWh*	37,11	*$/MWh*	0,0204	$kgCO_2/kWh$
G_{21}	0,629	*MWh*	0,001	*MWh*	35,92	*$/MWh*	0,0199	$kgCO_2/kWh$
G_{22}	0,169	*MWh*	0,001	*MWh*	35,68	*$/MWh*	0,0197	$kgCO_2/kWh$
G_{23}	0,398	*MWh*	0,002	*MWh*	35,80	*$/MWh*	0,0199	$kgCO_2/kWh$
G_{24}	0,339	*MWh*	0,001	*MWh*	35,77	*$/MWh*	0,0199	$kgCO_2/kWh$

Table 4 includes both grid electricity and CPC demands, where CPC demands are determined based on grid population density and corresponding facility allocation. Since PEM FCs are located both at central transformers and CPC sites, the same specifications are used, and no separate CPC-FC specific parameters are given in Table 2. The table also presents grid electricity supply costs, where the HSC network covers up to 40% of demand and the remaining 60% is supplied by the grid. These costs represent the delivery cost to end users, while emission values correspond to grid-based electricity. Electricty demand and purchased data are obtained from TEİAŞ [37], and emission data are sourced from Our World in Data (University of Oxford) [3].

 doi:10.20944/preprints202604.1696.v1

The electricity demand values in Table 4 correspond to 2023, while projections for 2025, 2030, and 2035 are obtained from the literature [45]. For 2035–2053, an average annual growth rate of 5.2% is adopted based on Türkiye's National Energy Plan-2022 by the Ministry of Energy and Natural Resources of Türkiye (MENR) [46]. Accordingly, Marmara Region electricity demand for 2023–2053 is projected and illustrated in Figure 9.

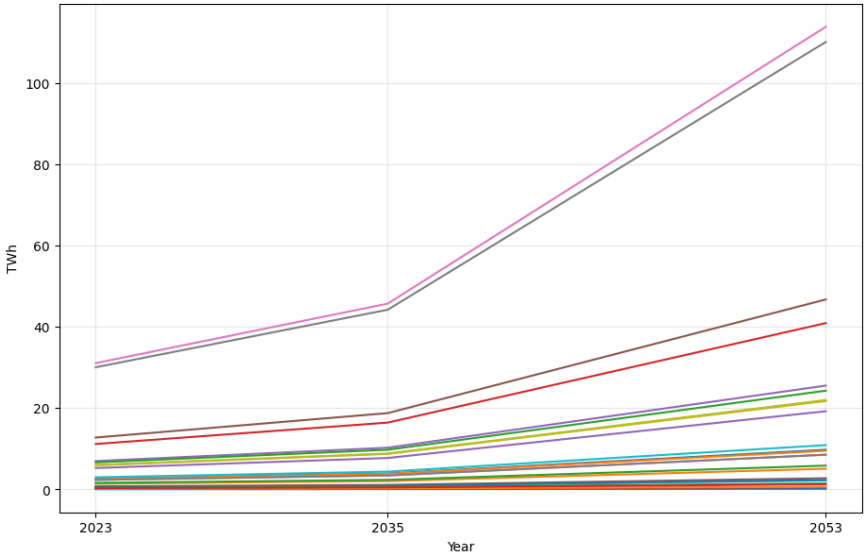

Figure 9. Grid demand projections, 2023-53.

Grid-level electricity demand is projected using a non-linear growth pattern: short-term changes follow observed step increases, while the 2035–2053 period is modeled using a smoothed average growth rate.

In addition to the parameters presented above, financial parameters are also collectively provided in Table 5.

Table 5. Financial parameters for HSC model [38–40].

Paramater	Production Tech						Storage Tech		FC Tech	Transport Modes*					
	SMR_g	SMR_b	COG	AEL	PEM	SOEC	CGH_2	LH_2	PEM	R_l	R_g	P_l	P_g	S_l	S_g
$CFRp_r$	0,094	0,094	0,089	0,102	0,117	0,117									
$CFRs_q$							0,094	0,089							
$CFRf_k$									0,117						
$CFRt_t$										0,132	0,149	0,083	0,083	0,089	0,094
Lp_r	25	25	30	20	15	15									
Ls_q							25	30							
Lf_k									15						
Lt_t										12	10	40	40	30	25
dr	0,08	0,08	0,08	0,08	0,08	0,08	0,08	0,08	0,08	0,08	0,08	0,08	0,08	0,08	0,08
Δ	3	3	3	3	3	3	3	3	3	3	3	3	3	3	3

*R_l: Road_liq, R_g: Road_gas, P_l: Pipeline_liq, P_g: Pipeline_gas, S_l: Sea_liq, S_g: Sea_gas.

In addition to the parameters presented above, three scenario-based parameters are externally provided to the model. These include "ζ_ω^β" representing the H_2 share (10%, 20%, 30%, 40); "η_ω^β" representing efficiency (1.00, 0.95, 0.90); and "dis_ω^β" representing the disaster condition (0, 1), resulting in a total of 24 scenario combinations. In addition, the availability parameters of the facilities, namely "aPR_ω, aST_ω, and aFC_ω" vary between 0.70 and 1.00 and are also externally assigned to the model according to these 24 scenarios.

In this context, the outputs of the single-period and multi-period models constructed based on the above model and data are presented in the following subsection.

 doi:10.20944/preprints202604.1696.v1

4.3. Model Outputs

In this section, the outputs of the single-period and multi-period models are presented. Since these outputs involve a high level of detail, only summarized results are provided, along with their detailed interpretations in this section and the Discussion section. In this context, rather than presenting separate tables for production, storage, and FC flow values for each node in the single-period model results, it is more appropriate to represent these flows on a map and provide aggregated values.

The proposed MILP model was implemented in Python using Pyomo and solved with the Gurobi optimizer. All computations were performed on a computer with an Intel i7-10750H CPU (2.60 GHz) and 16 GB RAM. The resulting single-period MILP model is large-scale, comprising 802,015 decision variables (798,312 continuous and 3,703 binary) and 730,967 constraints, with approximately 2.54 million nonzero elements.

Figure 10 shows the network flow on a map based on the aggregated outcome of all scenarios in the single-period stochastic model.

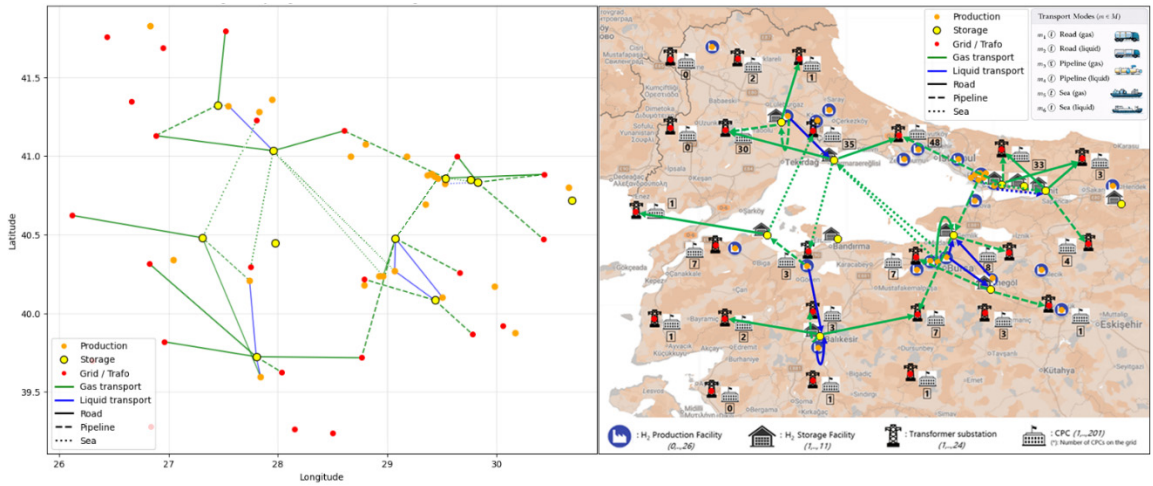

Figure 10. HSC network on the Marmara Region map / *Single-period model (2023).*

Figure 10 presents the MILP-based solution obtained using Python of the single-period model on the left and its representation on the actual regional map on the right. As shown on the map, gas transport is more prevalent than liquid transport, and road and pipeline modes are preferred over sea transport. This is partly because the sea area is more limited than the land area. The selected facilities include 6 AEL and 3 SMR_grey production facilities, and 8 CGH_2 storage units. According to stochastic model results, approximately 25% of the regional electricity demand is supplied by the HSC network, while detailed numerical results are provided in the tables below.

Since presenting production–storage–grid H_2 flows in terms of quantities, costs, and emissions for each node would result in overly detailed tables, aggregated values are reported instead. It should also be noted that quantities decrease across node due to transmission losses. Accordingly, Table 6 presents the aggregated flows.

Table 6. HSC network flows / *Single-period model output (2023).*

Indicator *All scenarios' aggregated outcome* *	**Locations & Techs & Flows**																		
	Grid (*g*)	**CPC (*c*)**	**Production Tech (*r*)**							**Storage Tech (*q*)**	**FC Tech (*k*)**	**Transport Modes* (*t*)**							**TOTAL**
			SMR_g	SMR_b	COG	AEL	PEM	SOEC	CGH_2	LH_2	PEM	R_l	R_g	P_l	P_g	S_l	S_g	i→s	s→k,g	k,g→c	

 doi:10.20944/preprints202604.1696.v1

Opened locations	16	201	3	0	0	6	0	0	8	0	217	-	-	-	-	-	-	-	-	-	-
Opened routes-i,s	-	-	-	-	-	-	-	-	-	-	-	7	3	0	4	2	3	-	-	-	19
Opened routes-s,k	-	-	-	-	-	-	-	-	-	-	-	4	10	0	11	0	1	-	-	-	26
Opened routes-k,c	-	-	-	-	-	-	-	-	-	-	-	168	84	0	0	0	0	-	-	-	252
Production amount-*Mt/y*	-	-	0,6	0	0	1,4	0	0	-	-	-	-	-	-	-	-	-	-	-	-	2
Production FOPEN-*MU/y*	-	-	877,8	0	0	1.672	0	0	-	-	-	-	-	-	-	-	-	-	-	-	2.550
Production FOPEX-*MU/y*	-	-	3,39	0	0	547,8	0	0	-	-	-	-	-	-	-	-	-	-	-	-	551,9
Production VOPEX-*MU/y*	-	-	603,4	0	0	1.684	0	0	-	-	-	-	-	-	-	-	-	-	-	-	2.288
Production ems-*MtC/y*	-	-	3,12	0	0	0,14	0	0	-	-	-	-	-	-	-	-	-	-	-	-	4.968
Storage amount-*Mt/y*	-	-	-	-	-	-	-	-	1,94	-	-	-	-	-	-	-	-	-	-	-	1,94
Storage FOPEN *MU/y*	-	-	-	-	-	-	-	-	400	-	-	-	-	-	-	-	-	-	-	-	400
Storage FOPEX *MU/y*	-	-	-	-	-	-	-	-	155,1	-	-	-	-	-	-	-	-	-	-	-	155,1
Storage ems-*MtC/y*	-	-	-	-	-	-	-	-	0,041	-	-	-	-	-	-	-	-	-	-	-	19,4
FC cnv-*MtH₂/y*	-	-	-	-	-	-	-	-	-	-	1,94	-	-	-	-	-	-	-	-	-	1,94
FC FOPEN-*MU/y*	-	-	-	-	-	-	-	-	-	-	8	-	-	-	-	-	-	-	-	-	8
FC FOPEX-M*U/y*	-	-	-	-	-	-	-	-	-	-	13,7	-	-	-	-	-	-	-	-	-	13,7
FC conversion emission -*MtC/y*	-	-	-	-	-	-	-	-	-	-	0,02	-	-	-	-	-	-	-	-	-	159
CPC-FC FOPEN *MU/y*	-	-	-	-	-	-	-	-	-	-	100,5	-	-	-	-	-	-	-	-	-	100,5
CPC-FC FOPEX *MU/y*	-	-	-	-	-	-	-	-	-	-	172,5	-	-	-	-	-	-	-	-	-	172,5
H_2 flow amount-*x1000 t/y*	-	-	-	-	-	-	-	-	-	-	-	-	-	-	-	-	-	1.938,8	1.831,7	1.702	2
Flow losses amount-*x1000 t/y*	-	-	-	-	-	-	-	-	-	-	-	-	-	-	-	-	-	68,6	107,1	129,5	305,2
H_2 flow cost-*MU/y*	-	-	-	-	-	-	-	-	-	-	-	-	-	-	-	-	-	24,5	61,7	18,6	104,8
H_2 flow emission -*MtC/y*	-	-	-	-	-	-	-	-	-	-	-	-	-	-	-	-	-	0,012	0.073	0,032	0,117

				unit	rate				
24,82%	HSC	**TOTAL***MWh/y*	33.813.780	**183,27**	**3,88**	*100%*	**TOTAL** electricity	*MWh/y*	**136.236.019**
	HSC	**TOTAL***MU/y*	6.197,2	*(U/MWh)*					
75,18%	PG	**TOTAL***MWh/y*	102.422.239	**47,19**					
	PG	**TOTAL***MU/y*	4.833,2	*(U/MWh)*		*100%*	**TOTAL** cost	*MU/y*	**11.030.33**
	HSC	**TOTAL***MWh/y*	33.813.780	**101,7**					
	HSC	**TOTAL***MtC/y*	3,44	*(kgC/MWh)*	**0,16**				
	PG	**TOTAL***MWh/y*	102.422.239	**644**		*100%*	**TOTAL** emission	*MtC/y*	**69,4**
	PG	**TOTAL***MtC/y*	65,96	*(kgC/MWh)*					

*ems: emission, *t/y*: ton/year, M*U/y*: million USD/year, *tC/y*: ton CO_2/year, *MtH₂/y*: million ton H_2/year.

Table 6 presents the aggregated results of the 24-scenario, two-stage stochastic single-period model, including flow quantities, costs, and emissions across production, storage, grid, and CPC nodes. These indicators are evaluated at both the system and facility levels, and transportation modes are analyzed based on route selections. Cost components are disaggregated into fixed opening, fixed operating, and variable operating costs to improve transparency.

First-stage decisions of the two-stage model—those independent of the scenario index ω and remaining active once selected—such as location choices, production and storage technology selections, and transportation mode decisions, are presented numerically in Table 6, while second-stage decisions are reported as aggregated outcomes across scenarios. The HSC network operates under different usage levels (10–40%), leading to an overall penetration rate of 24.82%.

An important point concerns the treatment of CPC facilities under disaster conditions. Since the disaster parameter takes binary values (0 or 1) across scenarios, CPC activation varies accordingly. However, to reflect a resilience-oriented planning perspective, all CPC facilities are assumed to be

 doi:10.20944/preprints202604.1696.v1

operational in the aggregated results. This assumption ensures system functionality under disruption scenarios and results in a conservative cost estimation.

The results indicate that AEL and SMR_g technologies dominate production decisions, while CGH_2 is selected for storage. Transportation mode diversity reflects geographical conditions, with road, pipeline, and maritime options used depending on distance and regional structure.

From a cost perspective, the grid supplies approximately 102.42 TWh/year (about 75% of total demand) with a total cost of approximately 4.83 billion USD, whereas the HSC network supplies 33.81 TWh/year (about 25%) with a total cost of approximately 6.2 billion USD. When normalized by electricity output, the unit costs are 47.19 USD/MWh for the grid and 183.27 USD/MWh for the HSC, corresponding to a cost ratio of approximately 3.88.

From an environmental perspective, the HSC accounts for only 4.95% of total emissions, producing approximately 3.44 $MtCO_2$/year, whereas the PG is responsible for 95.04% of emissions. Accordingly, the unit emission of the HSC is approximately 101.7 $kgCO_2$/MWh, compared to 644 $kgCO_2$/MWh for the grid, indicating that the HSC produces more than six times lower emissions per unit of electricity.

To examine how these system characteristics evolve over time, a multi-period model extending to 2053 is developed. The resulting facility evolution and cost dynamics are presented in Tables 7 and 8, respectively.

Table 7. Facilities opened over periods - *multi-period model / VNS solution / 2023-53.*

Periods	**Grid**	**CPC**	**Production Tech (*r*)**					**Storage Tech (*q*)**		**FC Tech (*k*)**
(*β*)	**(*g*)**	**(*c*)**	SMR_g	SMR_b	COG	AEL	PEM	SOEC	CGH_2	LH_2	PEM
1	10	201	2	0	1	1	3	2	2	4	211
2	13	0	2	0	1	1	5	3	2	4	13
3	15	0	2	0	1	1	6	6	2	4	15
4	17	201	2	0	1	2	6	7	3	4	218
5	19	0	2	0	1	2	6	7	3	5	19
6	20	201	2	0	1	2	7	7	4	5	221
7	21	201	2	0	1	2	10	7	4	5	222
8	24	201	2	0	1	2	11	7	4	6	225
9	24	201	2	0	1	2	11	7	4	6	225
10	24	0	2	0	1	2	11	7	4	6	24

According to the single-period model results in Table 6, two production technolo-gies and one storage technology were selected, whereas in Table 7 these numbers increase to five production technologies and two storage technologies. Compared to the single-period results, the multi-period model exhibits a higher diversity of selected technologies, including additional production and storage options. This increase is primarily driven by the use of the VNS metaheuristic [47], which explores alternative solution configurations rather than focusing solely on extreme optimal points.

While established technologies such as AEL and SMR_g remain dominant in early periods, emerging technologies such as PEM and SOEC are increasingly adopted over time, reflecting their declining cost trends. Similarly, while both CGH_2 and LH_2 storage technologies are selected in the first period, the model continues to utilize both options in later periods. The role of different cost components (CAPEX, FOPEX, VOPEX, and FOPEN) in shaping these dynamics is further analyzed in the Discussion section.

Another observation in Table 7 is the activation of CPC facilities. It should be noted that in the multi-period model, disaster conditions are introduced exogenously in specific periods to analyze their impact on the system.

In this context, Table 8 illustrates how these facility and flow decisions affect cost and emission outcomes up to 2053.

 doi:10.20944/preprints202604.1696.v1

Table 8. Costs, Electricity & Emissions - *multi-period model / VNS solution / 23-53.*

Periods (β)	Efficiency (η_{ω}^{β})	HSC					PG				Disaster Situation			TOTAL COST ($mUSD$)
		Usage (%)	Amount (Mt)	Electricity (MWh)	Cost ($MUSD$)	Emission (MtC)	Usage (%)	Electricity (MWh)	Cost ($MUSD$)	Emission (MtC)	Disaster ($0/1$)	CPCs served	CPCs electricity (MWh)	
1	0.90	19,05	1,26	25.257.86	10.494,4	4,2	80,95	109.537.20	15.215,7	71,5	1	201	515.000	25.710,
2	0.90	21,31	1,46	29.864.00	9.228,2	4,3	78,69	110.260.30	15.298,6	72,0	0	0	0.00	24.526,
3	0.95	23,49	1,67	34.247.89	10.065,7	4,4	76,51	111.549.80	15.459,8	72,8	0	0	0.00	25.525,
4	0.95	25,51	1,89	38.291.85	10.278,3	4,5	74,49	113.334.70	15.689,3	73,9	1	201	515.000	25.967,
5	0.95	27,79	2,13	43.822.57	10.461,8	4,6	72,21	113.878.50	15.746,5	74,3	0	0	0.00	26.208,
6	1.00	29,76	2.39	48.438.86	11.023,2	4,6	70,24	115.552.70	15.959,6	75,4	1	201	515.000	26.982,
7	1.00	31,72	2.65	54.049.75	11.878,7	4,7	68,28	117.476.10	16.206,6	76,7	1	201	515.000	28.085,
8	1.00	34,00	2.96	60.291.46	12.177,1	4,8	66,00	118.042.70	16.266,1	77,1	1	201	515.000	28.443,
9	1.00	35,05	3.16	64.247.81	11.625,3	4,8	64,95	120.004.10	16.517,4	78,1	1	201	515.000	28.142,
10	1.00	34,62	3.25	66.050.05	11.717,5	4,9	65,38	124.758.40	17.151,9	81,5	0	0	0.00	28.369,

Based on Table 8, a forward-looking analysis of the HSC network can be conducted; however, it is first necessary to compare the results with the single-period model to evaluate the impact of methodological differences on costs and emissions. During this comparison, it should be noted that each period in the multi-period model represents three years, and therefore results are converted to an annual basis. Accordingly, it is essential to determine which cost components are incurred in the first year.

In this context, all FOPEN costs—representing production, storage, transportation, and FC installations—are incurred once in the first year. CAPEX costs, which depend on installed capacity, are annualized using the CRF; therefore, even if no additional capacity is added within the period, these costs are distributed evenly and divided by three. Similarly, FOPEX and VOPEX components recur annually and are also divided by three to obtain annualized first-year costs.

The results reveal clear long-term trends in both cost and environmental performance. The share of the HSC increases from approximately 19% in the initial period to about 35% in the final period, while electricity generation from the HSC shows a moderate increase. Although the total HSC cost rises only slightly - from approximately 10.3 million USD to 11.2 million USD - the unit cost decreases significantly from about 407 USD/MWh to 169 USD/MWh. Similarly, while total emissions increase moderately from 4.2 $MtCO_2$ to 4.9 $MtCO_2$ (approximately 16%), the unit emission decreases substantially from around 166 $kgCO_2$/MWh to 74 $kgCO_2$/MWh.

In contrast, the share of the PG declines from approximately 81% to 65%, while its total cost increases from 15.2 million USD to 17.15 million USD. Despite this increase, the unit cost remains almost unchanged, decreasing slightly from about 139 USD/MWh to 137.5 USD/MWh. Meanwhile, total emissions rise from 71.5 $MtCO_2$ to 81.5 $MtCO_2$ (approximately 14%), and unit emissions show a slight increase from approximately 652.7 $kgCO_2$/MWh to 653.3 $kgCO_2$/MWh.

These results indicate that as the role of the HSC expands, electricity production increases while both unit cost and unit emissions decrease. In contrast, although the share of the PG declines, its environmental performance does not improve, highlighting the long-term sustainability advantages of hydrogen-based systems.

Figure 11 illustrates the evolution of LCOH, along with the levelized cost of electricity for hydrogen-based and grid-based supply (LCOE_HSC and LCOE_PG), and the associated emission trends over the study periods..

 doi:10.20944/preprints202604.1696.v1

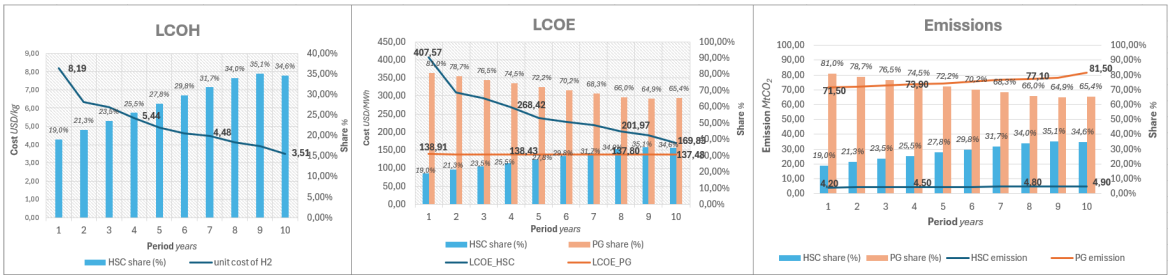

Figure 11. Unit costs, electricity & emissions - *multi-period model / VNS solution / 23-53.*

Figure 11 illustrates the evolution of cost and emission indicators over time. The results show a substantial reduction in hydrogen and hydrogen-based electricity costs, while grid electricity costs remain relatively stable.

In addition to cost reductions, the emission advantage of the HSC network remains significant throughout the planning horizon. While hydrogen utilization increases considerably, its emissions remain relatively low compared to the grid.

These findings highlight the long-term potential of hydrogen systems in energy transitions. A comprehensive evaluation of cost competitiveness, emission impacts, and technological drivers is presented in the Discussion section.

4.4. Sensitivity Analysis

The sensitivity of the proposed model is evaluated through its scenario-based structure and multi-period formulation. Instead of varying parameters individually, the model captures uncertainty and system response through predefined scenarios and temporal dynamics.

4.4.1. Single-Period Sensitivity Analysis

In the single-period model, sensitivity is evaluated through 24 scenarios defined by hydrogen share (ζ), transmission efficiency (η), and disaster conditions. Hydrogen share varies between 10% and 40%, directly affecting HSC utilization, while transmission efficiency captures losses in the supply chain and thus the effective energy delivered. Disaster conditions are modeled as a binary parameter, under which the system prioritizes CPC supply.

The results show that system performance responds systematically to parameter variations. The gap between planned and realized hydrogen supply is mainly driven by efficiency losses. For example, under a 30% target, reducing efficiency from 1 to 0.95 lowers the realized share to about 25%, and to around 20% at 0.9 efficiency. In disaster scenarios, fixed CPC demand (515,000 MWh) slightly increases the realized HSC share despite these losses.

These interactions create clear trade-offs between cost and emissions. Higher hydrogen shares improve environmental performance but increase system costs, whereas lower utilization or higher efficiency losses (e.g., ω6, ω9, ω22) reduce HSC costs while increasing reliance on grid electricity and emissions. A scenario-based band graph illustrating these relationships and the sensitivity behavior of the single-period model is presented in Figure 12.

 doi:10.20944/preprints202604.1696.v1

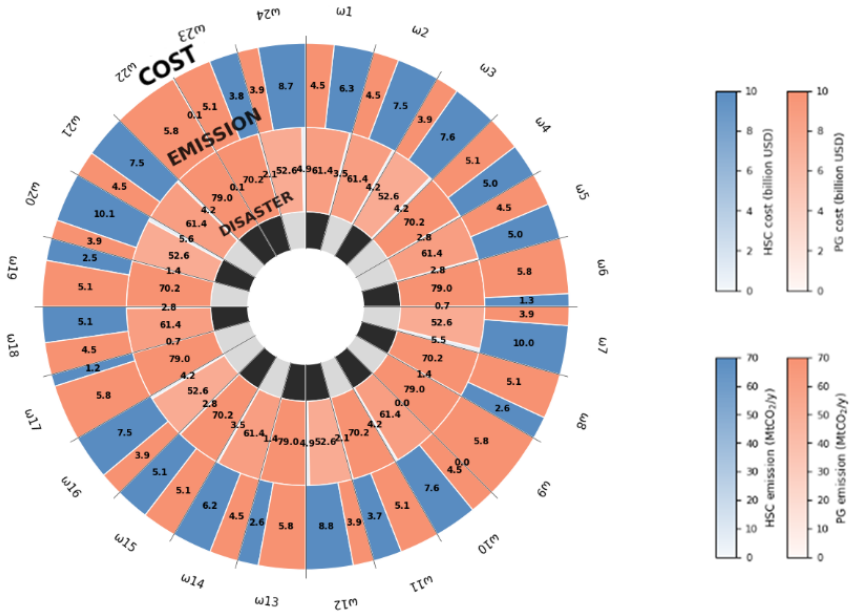

Figure 12. Scenario-based sensitivity analysis / *Single-period model.*

The band graph provides a layered representation of system performance across scenarios. The outer ring shows costs (blue for HSC, orange for PG), the middle ring shows emissions, and the inner ring indicates disaster conditions, with segment sizes reflecting proportional contributions.

As observed in Figure 12, the outer ring is generally dominated by blue tones, indicating higher HSC costs, while the middle ring is dominated by orange tones, showing that PG emissions exceed HSC emissions. This pattern highlights the fundamental trade-off between higher costs and lower emissions in hydrogen-based electricity.

Overall, the model exhibits consistent responses to parameter changes, without abrupt or unrealistic behavior. This indicates a stable structure in which hydrogen deployment enhances environmental performance but requires efficiency improvements and cost support. Furthermore, the prioritization of CPC demand highlights the role of hydrogen systems in strengthening energy system resilience.

For the single-period model, the sensitivity analysis is conducted on a scenario basis. In the following section, a more comprehensive version is presented, where the period-based sensitivity analysis extends the model across 10 periods, examining a total of 240 scenario–period combinations.

4.4.2. Multi-Period Sensitivity Analysis

In the multi-period model, sensitivity is evaluated over ten periods representing long-term system evolution rather than discrete scenario variations. The results reveal a gradual structural transition in both cost and emission patterns. As observed from Period 1 to Period 10, the dominance of HSC-related cost intensities weakens over time, indicating a continuous decline in hydrogen-based electricity costs. Nevertheless, PG unit costs remain relatively stable and, in most periods, still constitute a significant portion of the total cost structure.

A similar pattern can be observed in the emission layer. While HSC unit emissions remain consistently low and exhibit a slight decreasing trend, PG emissions continue to dominate due to their inherently higher emission intensity. This highlights that, although hydrogen systems provide clear environmental advantages, the overall emission structure of the system is still largely influenced by the conventional grid, especially in earlier periods.

These trends can be explained by the dynamic structure of the multi-period model. As shown in Table 7, the number of RES-based hydrogen production facilities increases over time, reflecting technological improvements and enhanced economic feasibility. In addition, parameters such as

 doi:10.20944/preprints202604.1696.v1

efficiency improvements, capital recovery factor (CRF), depreciation, and long-term financial assumptions contribute to the gradual reduction in HSC unit costs. The expansion of storage and fuel cell capacities further supports this transition by enabling a more effective integration of hydrogen into the electricity system.

The interaction of these factors results in a more balanced cost structure over time, while maintaining the environmental superiority of hydrogen-based electricity. The period-based cost and emission behavior of the system is illustrated in Figure 13.

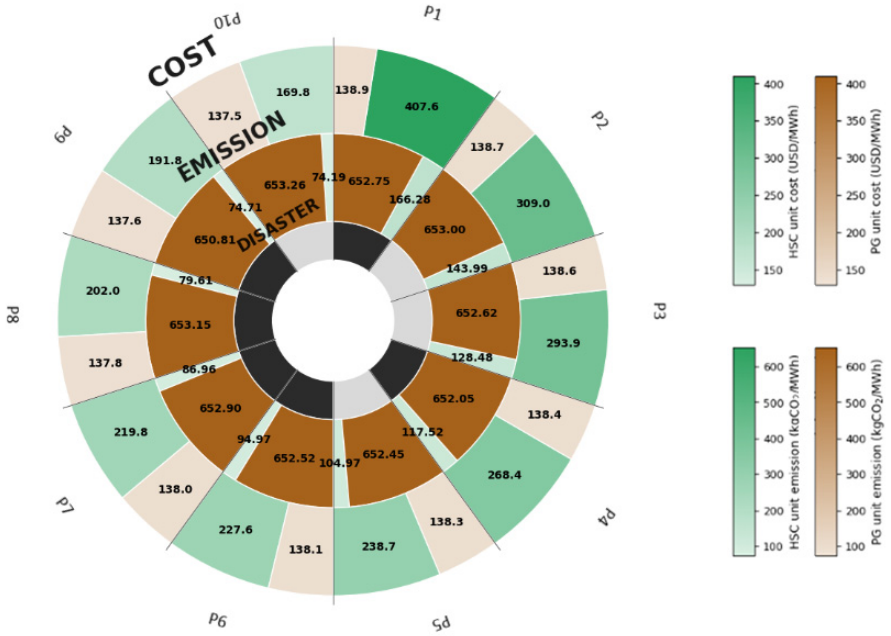

Figure 13. Period-based sensitivity analysis / *Multi-period model.*

Overall, the multi-period sensitivity analysis indicates that the hydrogen supply chain becomes increasingly competitive over time. While conventional grid electricity continues to dominate in terms of cost and emissions in the early periods, the gap narrows significantly in later periods, suggesting a favorable long-term outlook for hydrogen-based electricity systems in terms of both economic viability and environmental performance.

5. Discussion

The results demonstrate that hydrogen can play a meaningful role in regional electricity supply, although it remains cost-disadvantageous in the short term. In the single-period model, the HSC supplies approximately 24.82% of total electricity demand, corresponding to 33.81 TWh/year, while the grid supplies 102.42 TWh/year (about 75% of total demand). From a cost perspective, the grid incurs a total cost of approximately 4.83 billion USD, whereas the HSC reaches around 6.2 billion USD despite its lower share. When normalized by electricity output, this results in unit costs of 183.27 USD/MWh for hydrogen-based electricity and 47.19 USD/MWh for the grid, corresponding to a cost ratio of approximately 3.88.

From an environmental perspective, however, the results indicate a strong advantage for hydrogen systems. The HSC accounts for only 4.95% of total emissions, producing approximately 3.44 $MtCO_2$/year, while the grid is responsible for 95.04% of emissions. This leads to a unit emission of about 101.7 $kgCO_2$/MWh for the HSC, compared to 644 $kgCO_2$/MWh for the grid, indicating that hydrogen-based electricity produces more than six times lower emissions per unit of output. From a sustainability perspective, these findings highlight a clear trade-off between short-term economic efficiency and long-term environmental benefits.

 doi:10.20944/preprints202604.1696.v1

However, the multi-period results presented in Table 8 reveal a significantly different long-term trajectory. The HSC share increases from approximately 19.05% in the initial period to 34.62% in 2053, while the grid share declines from 80.95% to 65.38%. Despite this expansion, the total HSC cost increases only slightly—from approximately 10.3 billion USD to 11.2 billion USD—while its unit cost decreases sharply from about 407 USD/MWh to 169 USD/MWh. At the same time, Figure 11 shows that both LCOH and LCOE trends follow a clear downward path, indicating that cost reductions are primarily driven by technological progress and capital cost declines.

In contrast, the power grid exhibits a more rigid structure. Although its share decreases over time, total costs increase from approximately 15.2 billion USD to 17.15 billion USD, while unit costs remain nearly constant, declining only marginally from about 139 USD/MWh to 137.5 USD/MWh. Similarly, total emissions increase from approximately 71.5 $MtCO_2$ to 81.5 $MtCO_2$, whereas unit emissions remain almost unchanged at around 653 $kgCO_2$/MWh. These results indicate that, unlike the HSC, the power grid does not achieve significant improvements in unit performance over time. Overall, as the role of hydrogen expands, it enables simultaneous reductions in both unit cost and emissions, highlighting its long-term economic and environmental potential despite initial cost disadvantages. To provide a clearer comparison, the results of the single-period and multi-period models are jointly presented in Table 9.

Table 9. Cost–Emission comparison – *single & multi-period model / 23-53.*

		SINGLE-PERIOD OUTPUTS				MULTI-PERIOD OUTPUTS			
		Emission		Cost		Emission		Cost	
		Unit (*kgC/MWh*)	Total (*MtC/y*)	Unit (*USD/MWh*)	Total (*MUSD/y*)	Unit (*kgC/MWh*)	Total (*MtC/y*)	Unit (*USD/MWh*)	Total (*MUSD/y*)
2023	HSC	101,67	3,44	183,27	6.197,16	166,28	4,20	407,57	6.648,14
	PG	644,00	65,96	47,19	4.833,17	652,75	71,50	138,91	5.071,89
2053	HSC	-	-	-	-	74,90	4,90	169,83	7.042,20
	PG	-	-	-	-	653,26	81,50	137,48	5.717,31

Since the single-period model evaluates only the base year (2023), the first period of the multi-period model is taken as the reference for comparison. However, as each period in the multi-period structure represents three years, cost values must be adjusted to ensure comparability.

For the PG, which represents externally purchased electricity, costs can be directly converted to annual values by dividing by three. In contrast, this simplification does not fully apply to the HSC due to its investment-driven cost structure. Therefore, economic factors such as depreciation and the CRF are considered. In this context, CAPEX, VOPEX, and FOPEX are evaluated on a yearly basis, whereas FOPEN costs are assumed to occur entirely in the initial year, reflecting upfront investment decisions.

Under these assumptions, the total HSC cost is approximately 6.197 billion USD in the single-period model, compared to about 6.648 billion USD for the first period of the multi-period model. This difference can also be attributed to the solution methodologies. While the MILP model identifies an exact optimal solution, the VNS metaheuristic explores a broader solution space and converges to near-optimal solutions. As a result, the multi-period model yields slightly higher cost values than its single-period counterpart, as observed in Table 9.

In addition, Table 9 shows that in the initial year, HSC costs and emissions are higher than those of the grid. This is mainly due to the continued use of conventional production technologies, such as SMR-based pathways. However, the long-term results indicate a reversal of this trend. By 2053, HSC unit costs decrease significantly and approach grid-level costs, while emissions are substantially reduced. In contrast, grid costs either increase or remain relatively stable, and emissions persist at high levels. The fact that these outcomes are obtained under a system in which the share of HSC increases while the share of the grid declines further reinforces the long-term feasibility of hydrogen-based systems.

 doi:10.20944/preprints202604.1696.v1

A key structural difference emerges between the single-period MILP solution and the multi-period VNS solution. As shown in Table 6, the MILP framework concentrates on a limited set of technologies—primarily AEL and SMR_g for production and CGH_2 for storage—reflecting the tendency of exact optimization methods to select extreme optimal configurations. In contrast, Table 7 demonstrates that the VNS-based solution introduces a broader range of technologies, including COG, PEM, and SOEC, particularly in later periods. This diversification supports long-term sustainability by enabling technological transition pathways rather than locking the system into a narrow set of solutions, even though it leads to higher initial costs—evident from the first-period cost ratio of 5.68 derived from Table 8.

A more detailed examination of the technology evolution further clarifies the underlying cost dynamics. As indicated in Table 7, while AEL and SMR_g remain stable across periods, emerging technologies such as PEM and SOEC are increasingly adopted. This trend is consistent with Figure 8, which shows that these technologies exhibit the fastest decline in LCOH over time. Although LCOH is influenced by FOPEN, FOPEX, VOPEX, and CAPEX, the results confirm that CAPEX is the dominant driver of long-term cost reductions. FOPEN represents one-time investment costs and remains relatively stable, while FOPEX and VOPEX have comparatively moderate impacts. In contrast, CAPEX—strongly influenced by capacity expansion decisions and the CRF mechanism—plays a decisive role in shaping long-term cost trajectories.

Among these technologies, PEM stands out due to its relatively lower CAPEX, which explains its increasing adoption in later periods. Similarly, both CGH_2 and LH_2 storage technologies remain active throughout the planning horizon, indicating sustained storage diversification. In addition, the activation of CPC facilities in specific periods—introduced through disaster scenarios—demonstrates how system design is adapted to resilience requirements. The combined effect of these transitions is reflected in Table 8, where both cost reductions and improved emission outcomes are observed over time.

From an environmental sustainability perspective, the advantages of hydrogen are even more pronounced. Grid-related emissions remain significantly higher than HSC emissions throughout the planning horizon. Despite the increasing share of hydrogen, its emission levels remain relatively stable or decline, indicating a transition toward cleaner production technologies. In contrast, grid emissions increase despite a declining share, highlighting the limitations of conventional electricity systems in achieving deep decarbonization.

Geographical and infrastructural factors also play a significant role in shaping system design. As indicated in Table 6, the coexistence of road, pipeline, and maritime transportation modes reflects the spatial characteristics of the Marmara Region. Short-distance deliveries, particularly to CPC nodes, favor road transport, while pipeline transport becomes more efficient over longer distances. Maritime transport emerges as a viable option due to the central positioning of the sea within the region. This multimodal structure enhances operational flexibility and contributes to the overall sustainability of the hydrogen supply chain.

The inclusion of CPC nodes and disaster scenarios further strengthens the sustainability dimension of the model by incorporating system resilience. Hydrogen-based electricity can operate independently of grid infrastructure and ensure electricity supply to critical public centers, even under disruption conditions.

Despite these contributions, several limitations should be acknowledged. First, the projected cost reductions depend on assumptions regarding technological progress, particularly for emerging technologies such as PEM and SOEC. Second, although hydrogen is often treated as a low-emission energy carrier, the results remain sensitive to the selected production pathways. Third, resource constraints, especially water availability for electrolysis, are not explicitly modeled. Finally, real-world energy systems may deviate from modeled trajectories due to economic or geopolitical disruptions.

From a policy perspective, the results indicate that hydrogen-based systems are likely to require targeted support mechanisms during early deployment stages. Instruments such as investment

 doi:10.20944/preprints202604.1696.v1

subsidies, carbon pricing, or long-term purchase agreements could help improve economic feasibility. At the same time, the strong emission advantage of hydrogen suggests that environmental considerations alone may justify its earlier adoption.

The inclusion of CPC nodes and disaster scenarios further highlights the role of hydrogen in enhancing system resilience. Accordingly, policy frameworks that incorporate resilience alongside economic and environmental criteria may provide a more comprehensive basis for energy planning.

The long-term cost projections obtained in this study are also consistent with existing policy documents and the literature. According to the MENR Hydrogen Strategy and Roadmap [32], the expected levelized cost of hydrogen (LCOH) is projected to reach approximately 3.5 USD/kg by 2053. The results of this study yield a comparable value of about 3.51 USD/kg in the final period, indicating strong alignment with national projections.

Similarly, international studies such as those by the International Energy Agency [38] and the International Renewable Energy Agency [39] report that green hydrogen costs may decline to the range of 2–4 USD/kg by 2050 under favorable technological and market conditions. The findings of this study fall within this range, supporting the plausibility of the modeled cost trajectories.

This consistency with both national roadmaps and international projections strengthens the validity of the model outcomes and suggests that the proposed framework can produce realistic long-term estimates despite inherent uncertainties.

6. Conclusions

This study developed a stochastic, multi-period hydrogen supply chain (HSC) network model to evaluate the economic and environmental feasibility of hydrogen-based electricity generation in the Marmara Region. The single-period results indicate that hydrogen can supply approximately one-quarter of regional electricity demand, albeit at significantly higher costs compared to conventional grid electricity. Despite this cost disadvantage, hydrogen systems demonstrate a strong environmental advantage due to their near-zero emission profile.

The multi-period analysis provides a more comprehensive sustainability perspective by capturing long-term technological and economic dynamics. The results show that hydrogen costs decrease substantially over time, while its contribution to electricity supply increases from approximately 19% to 35%. This indicates that hydrogen systems gradually improve their economic sustainability and move closer to cost competitiveness, driven primarily by reductions in capital costs and technological advancements.

In addition to economic and environmental dimensions, the model incorporates system resilience through the integration of disaster scenarios. The findings demonstrate that hydrogen-based systems can ensure electricity supply to critical public centers under grid failure conditions, highlighting their role in enhancing the resilience component of sustainability. This multi-dimensional perspective - combining economic feasibility, environmental performance, and system resilience - positions hydrogen as a promising component of future sustainable energy systems.

From a broader perspective, the results suggest that hydrogen should be considered a complementary rather than a substitutive solution in energy transitions. While its short-term economic limitations remain significant, its long-term sustainability potential becomes increasingly evident as technological progress reduces costs and improves system performance. Therefore, policy support, technological innovation, and infrastructure development are essential to accelerate this transition.

Future research may extend this study by incorporating renewable energy integration, resource constraints such as water availability, and policy mechanisms including carbon pricing. In addition, hybrid solution approaches that combine exact optimization and metaheuristic methods may improve solution quality for large-scale problems.

Supplementary Materials: The following supporting information can be downloaded at the website of this paper posted on Preprints.org.

 doi:10.20944/preprints202604.1696.v1

Author Contributions: Conceptualization, A.Z.S., S.S.K. and S.I.S.; methodology, A.Z.S; software, A.Z.S; validation, S.S.K. and S.I.S.; formal analysis, A.Z.S.; investigation, A.Z.S, S.S.K. and S.I.S.; resources, A.Z.S.; data curation, A.Z.S.; writing—original draft preparation, A.Z.S.; writing—review and editing, S.S.K. and S.I.S.; visualization, A.Z.S.; supervision, S.S.K. and S.I.S.; project administration, S.S.K. and S.I.S; All authors have read and agreed to the published version of the manuscript.

Funding: This research received no external funding.

Institutional Review Board Statement: Not applicable.

Informed Consent Statement: Not applicable.

Data Availability Statement: The necessary data to test the study are provided within the article.

Acknowledgments: The authors would like to acknowledge that this paper is submitted in partial fulfillment of the requirements for the Ph.D. degree at Yildiz Technical University. This work was supported by the İlim Yayma Foundation.

Conflicts of Interest: The authors declare no conflicts of interest.

Appendix A

Appendix A.1

Table A1. Sets of the mathematical model with definitions.

NoSets		Definition	NoSets		Definition
1	$\beta \in B$: {1,2,...,10}	Set of planning periods (2023–53)	**8**	$k \in K$: {1,2,...,225} $k \in K^g \wedge k \in K^c$ $K^g \subset K \wedge K^c \subset K$ $K = K^c \cup K^g$, $K^c \cup K^g = \emptyset$	Set of candidate FC units, each associated with a physical location. (K^g for grid-side, K^c for CPC-side)
2	$\omega \in W$: {1,2,...,24}	Set of scenarios			
3	$i \in I$: {1,2,..,26}	Set of production nodes			
4	$s \in S$: {1,2,...,11}	Set of storage nodes			
5	$g \in G$: {1,2,...,24}	Set of grid (transformer) nodes	**9**	$c \in C$: {1,2,...,201}	Set of CPC nodes
6	$r \in R$: {1,2,...,6}	Set of production technologies	**10**	$t \in T$: { T^{road}, T^{pipe}, T^{sea} } T^{road} = {road_liq,road_gas} T^{pipe} = {pipe_liq, pipe_gas} T^{sea} = {sea_liq, sea_gas} $T^{road} \cup T^{pipe} \cup T^{sea}$, $T^{road} \cap T^{pipe} \cap T^{sea} =$	Set of hydrogen transport modes
7	$q \in Q$: {1,2}	Set of storage technologies			

To elaborate on the explanations provided in Table A1, the sets and indices of the model can be detailed as follows:

- The period index β represents a multi-period structure of 10 periods, each covering three years, corresponding to a 30-year planning horizon aligned with Türkiye's 2053 targets and international benchmarks such as the IEA 2050 vision.
- The scenario index ω captures uncertainty through combinations of three parameters: ζ_{ω}^{β} (four levels, HSC share), η_{ω}^{β} (three levels, transmission efficiency), and dis_{ω}^{β} (two levels, disaster status), resulting in 24 scenarios.
- The spatial indices i, s, g, k, and c correspond to production sites, storage facilities, grid regions, FCs, and CPCs, respectively. Their geographical locations are presented in detail under the Application section and visualized on the regional grid map.
- The production technology index r includes six alternative hydrogen production technologies. Three are conventional-based technologies: Coal gasification (COG), Steam methane reforming (SMR_grey), and blue steam methane reforming (SMR_blue). The remaining three are renewable energy source (RES)-based electrolysis technologies: Proton exchange membrane (PEM), alkaline electrolysis (AEL), and solid oxide electrolysis cell (SOEC).
- The storage technology index q consists of two alternatives: Compressed gaseous hydrogen (CGH_2) and liquid hydrogen (LH_2).

 doi:10.20944/preprints202604.1696.v1

- The transportation technology index t includes six modes: liquid road, gaseous road, liquid pipeline, gaseous pipeline, liquid sea and gaseous sea.
- The FC index k comprises a total of 225 units, of which 24 are integrated with grid transformer substations and 201 are located adjacent to CPCs.

Table A3. Parameters of the mathematical model with definitions.

No	Parameters	Definition	No	Parameters	Definition
	Scenarios & Policy		**27**	cxF_q^β	CAPEX coefficient of the FC unit installed at candidate site k in period β (USD/kW).
1	$prob_\omega$	Probability of scenario ω.		*Capacity (Tech-Perf.)*	
2	ζ_ω^β	Target share of H2-based electricity in total grid demand under scenario ω during period β.	**28**	$CapP_r^\beta$	Annual hydrogen production capacity of technology r in period β (ton/year per site).
3	η_ω^β	Transmission/delivery efficiency factor under scenario ω during period β.	**29**	$CapS_s^\beta$	Annual hydrogen storage capacity of technology q in period β (ton/year per site).
4	dis_ω^β	Binary parameter indicating disaster occurrence under scenario ω in period β.	**30**	$CapF_k^\beta$	Annual electricity generation capacity of one FC unit in period β (MWh/year per site).
	Demand & Grid		**31**	α^β	Hydrogen-to-electricity conversion factor in period β (MWh per ton H_2).
5	DG_ω^β	Electricity demand at grid node g during period β.	**32**	aPR_ω	Production capacity availability factor under scenario ω.
6	DC_ω^β	Electricity demand at CPC node c during period β (MWh/year).	**33**	aST_ω	Storage capacity availability factor under scenario ω.
7	cGR_ω^β	Unit cost of PG electricity at node g in period β (USD/MWh).	**34**	aFC_ω	FC capacity availability factor under scenario ω.
	Prod. Tech- Cost			*Inventory*	
8	fnP_r^β	Fixed opening expenditure (FOPEN) of production technology r in period β (USD/site).	**35**	$InvO_s$	Initial hydrogen inventory at storage node s at the beginning of the planning horizon (ton).
9	fxP_r^β	Fixed operating expenditure (FOPEX) of production technology r in period β (USD/site-year).	**36**	hcS_q^β	Inventory holding cost for storing hydrogen using storage technology q during period β (USD/ton-period).
10	vP_r^β	Variable operating expenditure (VOPEX) of hydrogen production using technology r in period β (USD/tonH_2).	**37**	bo_q^β	Hydrogen loss fraction (boil-off/leakage) for storage technology q during period β
11	cxP_r^β	Capital expenditure (CAPEX) coefficient for production technology r in period β (USD/site).	**38**	SS_s^β	Minimum safety stock requirement at storage node s in period β (ton).
	Stor. Tech- Cost		**39**	pSO	Penalty coefficient for storage stockout (USD/ton).
12	fnS_q^β	FOPEN of storage technology q in period β (USD/site)		*Emission*	
13	fxS_q^β	FOPEX of storage technology q in period β (USD/site-year).	**40**	$efGR_\omega^\beta$	Emission factor of electricity purchased from the external PG at node g during period β (tCO_2 per MWh).
14	cxS_q^β	CAPEX coefficient for storage technology q in period β (USD/site).	**41**	efP_ω^β	Greenhouse gas emission factor of hydrogen production technology r during period β (tCO_2 per ton H_2).
	Transport		**42**	$efTR_t^\beta$	Emission factor associated with hydrogen transportation using mode t during period β (tCO_2 per ton-km).
15	cPS_t^β	Transport VOPEX for hydrogen shipments from production to storage using mode t in period β (USD/ton-km).	**43**	efF_k^β	Emission factor of electricity generated by the FC unit installed at site k during period β (tCO_2 per MWh).
16	cSK_t^β	Transport VOPEX for hydrogen shipments from storage to FC using mode t in period β (USD/ton-km).		*Financial*	
17	$fdPS_t^\beta$	Transport FOPEN per km for production-to-storage transport	**44**	dr	Annual discount rate

 doi:10.20944/preprints202604.1696.v1

		using mode t in period β (USD/km-year).			
18	$fdSK_t^{\beta}$	Transport FOPEN per km for storage-to-FC transport using mode t in period β (USD/km-year).	**45**	Δ	Length of one planning period in years (Δ=3).
19	$dPS_{i,s,t}$	Distance between production node i and storage node s using mode t (km).	**46**	DF^{β}	Discount factor applied to costs occurring in period β.
20	$dSK_{s,k,t}$	Distance between storage node s and FC k using mode t (km).	**47**	$Lp_r/Ls_q/Lf_k/Lt_t$	Economic lifetime of a production/stotage/FC/transport technologies (year)
21	dGC_{gc}	Distance between grid node g and CPC node c (km).	**48**	$CRFp_r/CRFs_q/CRFf_k/CRFt_t$	Capital recovery factor for production/stotage/FC/transport technologies
22	$\eta PS_t^{\beta}, \eta SK_t^{\beta}$	Effective hydrogen delivery factors for PS and SK transport links in period β, accounting for transport losses.		*Budget, Penalty, Node, Big-M*	
23	cxT_t^{β}	CAPEX coefficient of transportation mode t in period β (USD/km).	**49**	BD^{β}	Maximum available investment budget in period β (USD).
	FC Technology		**50**	λ	Weight coefficient applied to total emissions in the objective function.
24	fnF_k^{β}	FOPEN of installing one FC unit at candidate site k in period β (USD per site).	**51**	$pDG, pCPC, pZL, pZU$	Penalty coefficients associated with slack variables.
25	fxF_k^{β}	FOPEX of a FC unit installed at site k in period β (USD per site-year).	**52**	μ_{cg}	μ(cg) =1 if CPC c is associated with grid node g; 0 otherwise.
26	ηF_k^{β}	Fraction of hydrogen energy effectively converted into electricity by the FC in period β.	**53**	$MPS_{i,s,t}/MPS_{s,k,t}/Me$	Big-M constant that upper-bounds hydrogen flow between production node i/s and storage node s/k when transport mode t is selected (ton/year)/ Me: Big-M constant used to deactivate CPC electricity supply in non-disaster scenarios (MWh/year)

Table A4. Decision variables of the mathematical model with definitions.

No	Variables	Definition	No	Variables	Definition
1	$h_{i,r,\omega}^{\beta} \geq 0$	Amount of hydrogen produced at production node i using technology r under scenario ω during period β (ton/year).	**11**	$\gamma_{i,s,t}^{\beta} \in \{0,1\}$	Equals 1 if transport mode t is selected between production node i and storage node s in period β.
2	$x_{i,s,t,\omega}^{\beta} \geq 0$	Hydrogen flow transported from production node i to storage node s using transport mode t under scenario ω during period β (ton/year).	**12**	$\gamma_{s,k,t}^{\beta} \in \{0,1\}$	Equals 1 if transport mode t is selected between storage node s and FC site k in period β.
3	$y_{s,k,t,\omega}^{\beta} \geq 0$	Hydrogen flow transported from storage node s to FC site k using transport mode t under scenario ω during period β (ton/year).	**13**	$\psi_k^{\beta} \in \{0,1\}$	Equals 1 if a FC unit is installed at candidate site k in period β; 0 otherwise.
4	$z_{g,c,t,\omega}^{\beta} \geq 0$	Hydrogen transported from grid g to CPC c using transport mode $t \in T(road)$ road under scenario ω during period β (ton/year).	**14**	$slDG_{g,\omega}^{\beta} \geq 0$	Slack variable representing unmet grid electricity demand at node g.
5	$eF_{k,\omega}^{\beta} \geq 0$	Electricity generated by the FC unit installed at site k under scenario ω during period β (MWh/year).	**15**	$slCPC_{g,\omega}^{\beta} \geq 0$	Slack variable representing unmet CPC electricity demand associated with grid node g during disaster conditions.
6	$eGR_{k,g,\omega}^{\beta} \geq 0$	Electricity supplied from FC site $k \in K^g$ to grid node g under scenario ω during period β (MWh/year).	**16**	$slZL_{g,\omega}^{\beta} \geq 0$	Slack variable for hydrogen share lower bound violation.
7	$pGR_{g,\omega}^{\beta} \geq 0$	Electricity purchased from the external grid at grid node g under scenario ω during period β (MWh/year).	**17**	$slZU_{g,\omega}^{\beta} \geq 0$	Slack variable for hydrogen share upper bound violation.
8	$eCPC_{c,\omega}^{\beta} \geq 0$	The amount of electricity supplied to CPC c in scenario ω and period β(MWh/year).	**18**	$SO_{s,\omega}^{\beta} \geq 0$	Unmet hydrogen shortage at storage node s in period β under scenario ω (ton).
9	$\delta_{i,r}^{\beta} \in \{0,1\}$	Equals 1 if production technology r is installed at production node i in period β; 0 otherwise.	**19**	$Inv_{s,\omega}^{\beta} \geq 0$	End-of-period inventory equals previous inventory (reduced by storage losses), plus effective inflow from production.

 doi:10.20944/preprints202604.1696.v1

10	$\phi_{s,q}^{\beta} \in \{0,1\}$	Equals 1 if storage technology q is installed at storage node s in period β; 0 otherwise.

References

1. International Energy Agency. World Energy Outlook 2024; IEA: Paris, France, 2024.
2. International Energy Agency. Net Zero by 2050—A Roadmap for the Global Energy Sector; IEA: Paris, France, 2021.
3. Electricity Generation and Energy Consumption from Renewables. Available online: https://ourworldindata.org/grapher/electricity-renewables (accessed on 14 March 2024).
4. Shang, Y.; Han, D.; Gozgor, G.; Mahalik, M.K.; Sahoo, B.K. The impact of climate policy uncertainty on renewable and non-renewable energy demand in the United States. *Renewable Energy* **2022**, *197*, 654–667.
5. Das, A.; Jani, H.K.; Nagababu, N.; Kacchwaha, S.S. A comprehensive review of wind–solar hybrid energy policies in India: Barriers and recommendations. *Renewable Energy* **2020**, *35*, 108–121.
6. Şekerci, A.Z. Assessment of Future RES and CO2 Use of Türkiye and Other Countries in Terms of Climate Targets of International Agreements: An Estimate with ANFIS. *Sigma Journal of Engineering and Natural Sciences* **2026**, *(submitted; accepted; in press).*
7. International Energy Agency. Global Hydrogen Review 2025; IEA: Paris, France, 2025.
8. Li, F.; Liu, D.; Sun, K.; Yang, S.; Peng, F.; Zhang, K.; Guo, G.; Si, Y. Towards a Future Hydrogen Supply Chain: A Review of Technologies and Challenges. *Sustainability* **2024**, *16* (5), 1890.
9. Hugo, A.; Rutter, P.; Pistikopoulos, S.; Amorelli, A.; Zoia, G. Hydrogen infrastructure strategic planning using multi-objective optimization. *Int. J. Hydrogen Energy* **2005**, *30*, 1523–1534.
10. Kim, J.; Lee, Y.; Moon, I. Optimization of a hydrogen supply chain under demand uncertainty. *Int. J. Hydrogen Energy* **2008**, *33*, 4715–4729.
11. Almansoori, A.; Shah, N. Design and operation of a stochastic hydrogen supply chain network under demand uncertainty. *Int. J. Hydrogen Energy* **2012**, *37*, 3965–3977.
12. Zhang, Y.; Jiang, Y. Supply chain optimization of biodiesel produced from waste cooking oil. *Transp. Res. Procedia* **2016**, *12*, 938–949.
13. Ogumerem, G.S.; Kim, C.; Kesisoglou, I.; Diangelakis, N.A.; Pistikopoulos, E.N. A multi-objective optimization for the design and operation of a hydrogen network for transportation fuel. *Chem. Eng. Res. Des.* **2018**, *131*, 279–292.
14. Woo, Y.B.; Cho, S.; Kim, J.; Kim, B.S. Optimization-based approach for strategic design and operation of a biomass-to-hydrogen supply chain. *Int. J. Hydrogen Energy* **2016**, *41*, 5405–5418.
15. da Silva, P.R.; Aragão, M.E.; Trierweiler, J.O.; Trierweiler, L.F. A systematic approach for flexible cost-efficient hydrogen network design for hydrogen management in refineries. *Chem. Eng. Res. Des.* **2021**, *172*, 53–70.
16. Ehrenstein, M.; Galán-Martín, Á.; Tulus, V.; Guillén-Gosálbez, G. Optimising fuel supply chains within planetary boundaries: A case study of hydrogen for road transport in the UK. *Appl. Energy* **2020**, *276*, 115486.
17. Almaraz, D.-L.; Rácz, V.; Azzaro-Pantel, C.; Szántó, Z.O. Multiobjective and social cost-benefit optimisation for a sustainable hydrogen supply chain: Application to Hungary. *Appl. Energy* **2022**, *325*, 119882.
18. Yu, Z.; Wu, X.; Wei, B.; Wang, H.; Sun, Y. Optimization of the future hydrogen supply chain for China. *Int. J. Hydrogen Energy* **2025**, *50*, 1860–1875.
19. Kamarudin, S.K.; Daud, W.R.W.; Yaakub, Z.; Misron, Z.; Anuar, W.; Yusuf, N.N.A.N. Synthesis and optimization of future hydrogen energy infrastructure planning in Peninsular Malaysia. *Int. J. Hydrogen Energy* **2009**, *34*, 2077–2088.
20. Guillén-Gosálbez, G.; Mele, F.D.; Grossmann, I.E. A bi-criterion optimization approach for the design and planning of hydrogen supply chains for vehicle use. *AIChE J.* **2009**, *56*, 650–667.
21. Johnson, N.; Ogden, J. A spatially-explicit optimization model for long-term hydrogen pipeline planning. *Int. J. Hydrogen Energy* **2012**, *37*, 5421–5433.
22. Won, W.; Kwon, H.; Han, J.-H.; Kim, J. Design and operation of renewable energy sources based hydrogen supply system: Technology integration and optimization. *Renew. Energy* **2017**, *10*, 226–238.

 doi:10.20944/preprints202604.1696.v1

23. Ayvaz, B.; Kuşakçı, A.O.; Öztürk, F.; Sırakaya, M. Biyodizel tedarik zinciri ağ tasarımı için çok amaçlı karma tam sayılı doğrusal programlama modeli önerisi. *Uludağ Univ. Müh. Fak. Derg.* **2018**, *23*, 55–70.
24. Talebian, H.; Herrera, O.E.; Mérida, W. Spatial and temporal optimization of hydrogen fuel supply chain for light duty passenger vehicles in British Columbia. *Int. J. Hydrogen Energy* **2019**, *44*, 25939–25956.
25. Li, L.; Manier, H.; Manier, M.-A. Integrated optimization model for hydrogen supply chain network design and hydrogen fueling station planning. *Comput. Chem. Eng.* **2020**, *134*, 106683.
26. Güler, M.G.; Geçici, E.; Erdoğan, A. Design of a future hydrogen supply chain: A multi period model for Turkey. *Int. J. Hydrogen Energy* **2021**, *46*, 16279–16298.
27. Forghani, K.; Al-Sharif, A.; Balfaqih, M.H. A multi-period sustainable hydrogen supply chain model considering pipeline routing and carbon emissions: The case study of Oman. *Renew. Sustain. Energy Rev.* **2023**, *180*, 114832.
28. Doniavi, A.; Babazadeh, M.; Hasanzadeh, A. Optimization of renewable energy supply chain for sustainable hydrogen energy production from plastic waste. *Sustainability* **2023**, *15*, 5832.
29. Ibrahim, H.; Al-Mohannadi, D. Optimization of low-carbon hydrogen supply chain networks in industrial clusters. *Int. J. Hydrogen Energy* **2023**, *48*, 12245–12260.
30. Sgarbossa, F.; Arena, U.; Tang, C.; Peron, M. Renewable hydrogen supply chains: A planning matrix and an agenda for future research. *Int. J. Prod. Econ.* **2023**, *255*, 108645.
31. Hou, J.; Xu, C.; Liu, J.; Wen, Z. Green Hydrogen Supply Chain Decision-Making and Contract Optimization Under Uncertainty: A Pessimistic-Based Perspective. *Sustainability* **2025**, *17*(13), 6181.
32. Republic of Türkiye Ministry of Energy and Natural Resources. *Türkiye Hydrogen Technologies Strategy and Roadmap*; Ministry of Energy and Natural Resources: Ankara, Türkiye, 2023.
33. Palubeckis, G.; Ostreika, A.; Platužienė, J. A Variable Neighborhood Search Approach for the Dynamic Single Row Facility Layout Problem. *Mathematics* **2022**, *10*, 2373.
34. Chen, Y.; Lou, P.; Jiang, W. Enhanced Variable Neighborhood Search-Based Recovery Supplier Selection for Post-Disruption Supply Networks. *Processes* **2021**, *9*, 670.
35. Organize Sanayi Bölgeleri Üst Kuruluşu (OSBÜK). Sayılarla OSB'ler: OSB Listesi. Available online: https://osbuk.org/view/sayilarlaosb/osbliste.php (accessed on 8 March 2026).
36. Istanbul34. Ports of the Marmara Region. Available online: https://www.istanbul34.com.tr/limanlar?port=marmara (accessed on 8 March 2026).
37. Türkiye Türkiye Elektrik İletim A.Ş. (TEİAŞ). Aylık Elektrik Üretim–Tüketim Raporları; TEİAŞ: Ankara, Türkiye.
38. IEA. *Global Hydrogen Review 2023*; International Energy Agency: Paris, France, 2023.
39. IRENA. *Global Hydrogen Trade to Meet the 1.5°C Climate Goal: Technology Review of Hydrogen Carriers*; International Renewable Energy Agency: Abu Dhabi, United Arab Emirates, 2022.
40. NREL. *Hydrogen Production Cost Analysis*; National Renewable Energy Laboratory: Golden, CO, USA, 2021.
41. U.S. DOE. *Hydrogen Shot: Hydrogen Energy Earthshot Initiative*; U.S. Department of Energy: Washington, DC, USA, 2022.
42. Zhang, Y.; Jiang, Y. Supply Chain Optimization of Hydrogen Energy Systems: A Review of Transportation and Infrastructure Design. *Int. J. Hydrogen Energy* **2017**, *42*, 13304–13323.
43. U.S. Department of Energy. *Hydrogen Delivery Scenario Analysis Model (HDSAM)*; DOE Hydrogen Program: Washington, DC, USA, 2020. Available online: https://www.hydrogen.energy.gov (accessed on 8 March 2026).
44. Agnolucci, P.; McDowall, W. Designing Future Hydrogen Supply Chains: Insights from Energy Systems Analysis. *Energy Policy* **2013**, *61*, 1077–1087.
45. Şekerci, A.Z.; Kara, S.S. An Application on Supplying Türkiye's Electricity Demand with Hydrogen: Demand Forecasting with ANFIS. In Industrial Engineering in the Era of Industry 5.0; Calisir, F.; Zaim, S.; Eryarsoy, E.; Durucu, M., Eds.; Springer: Cham, Switzerland, 2026; Proceedings of the Global Joint Conference on Industrial Engineering and Its Application Areas (GJCIE 2025), Istanbul, Türkiye, 12–15 August 2025.

 doi:10.20944/preprints202604.1696.v1

46. Republic of Türkiye Ministry of Energy and Natural Resources. Türkiye National Energy Plan 2023–2035; Ankara, Türkiye, 2022.
47. García, J.; Gómez, M.; López, A. Metaheuristic Optimization Techniques in Power Systems. Sustainability 2023, 15, 9434.